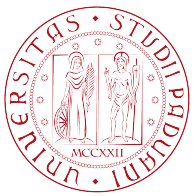

Università degli Studi di Padova

DIPARTIMENTO DI FISICA E ASTRONOMIA "GALILEO GALILEI"
Corso di Laurea in Fisica

Design of a plasma neutralizer for negative ion beam

Progetto di un neutralizzatore al plasma per fasci di ioni negativi

Candidato:
Luca Balbinot
Matricola 1069477

Relatore:
Dott. Gianluigi Serianni

Correlatore:
Dott. Emanuele Sartori

Anno Accademico 2015/2016

Contents

Introduction

Plasma, in fusion chambers, needs to be heated to reach fusion temperature. Traditional heating of thermonuclear fusion experiments are ohmic heating, by magnetic induction, and $^4He^{2+}$ (produced in fusion reaction) bremsstrahlung. Others additional heating systems are required, as sketched in figure 1. Among these, the injection of intense beams of energetic particles is very important, generally obtained by electrostatic acceleration of negative hydrogen ions. Ions selected are hydrogen and deuterium ions in order to heat the fusion plasma with the same elemens it is made of.

Ions are accelerated and collimated by electric fields, so reaching the energy

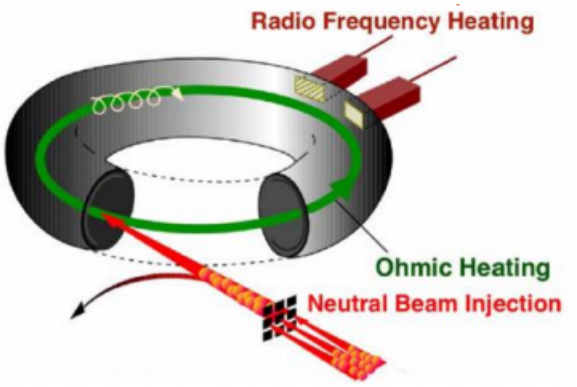

Figure 1: Sketch of different energy supplies to a tokamak [3]

required; then ions have to be neutralized before being injected in order to pass through the magnetic plasma confinement of the fusion chamber. This is the reason why negative ion beams are chosen as the precursor beam of neutral beam injectors (NBIs) instead of positive ion beams. Infact neutralization of a negative ion beams is much easier than that of positive ion beams [1].

Negative ion-based neutral beam injectors will play an important role in heating and driving a current of fusion plasma. As an example ITER [2] will be provided with three NBIs, two hydrogen NBIs and a deuterium one. The demonstration reactor DEMO will be provided with NBIs as well.

Neutral beam injectors can be divided in five parts: source of negative plasma particles, accelerator, neutralizer, separator, that discarts residual ions of the beam, and the duct going to the fusion chamber.[1]

Future fusion plants will require NBI with a high system efficiency, in order to reduce power dispersion and optimize power recycling.

NBI efficiency is determined mainly by the neutralization efficiency of the driven

[1] For high energy beams stripping cross sections are much bigger than electron capure ones[2].

[2] The next biggest reactor under construction in southern France

negative ion beams, that is the percentage of the primary beam neutralized in the neutralizer. The beam infact could not be completely neutralized, some of its power infact has to be discarted as H^- and H^+ beam fraction.
In the world the major research institutes studing Ion-based neutral beam injectos are: QST (Japan)[3], NIFS (Japan) [4], IPP (Germany)[5] and Consorzio RFX (Italy).
It was demonstrated that the neutralization efficiency of a neutral gas neutralizer is limited to $\simeq 60\%$ for the current high energy negative ion beams. [4] [5]
Plasma neutralizer instead should provide a higher neutralization efficiency of the primary negative ion beam [4] [5]. With generating a high density plasma in the neutralizer higher performances of the NBI are reached, efficiency of neutralization of DEMO plasma neutralizer is predicted to reach $\simeq 80\%$.
Nevertheless, costs, in terms of energy, of generation of high density plasma could be high enough to cancel the energetic benefits of the plasma neutralizer. [6] [7]
This thesis describes a method for using the plasma generated by the passage of the beam itself through a neutral gas neutralizer. The plasma required for higher neutralization efficiency will not be externally activated, requiring energy, but will be generated be the beam itself thanks to ionizing collisions with the background gas.
Thus, with the purpose of generating high density plasma, confinement of self generated plasma and neutral gas density have to be optimized.

0.1 NIO1

NIO1 (Negative Ion Optimization phase 1) [6] is a compact radio frequency ion source, installed at Consorzio RFX. It is designed to generate a 60 keV-130 mA hydrogen negative ion beam.[10]
In figure 2 a external view of NIO1 current source accelerator and neutralizer is

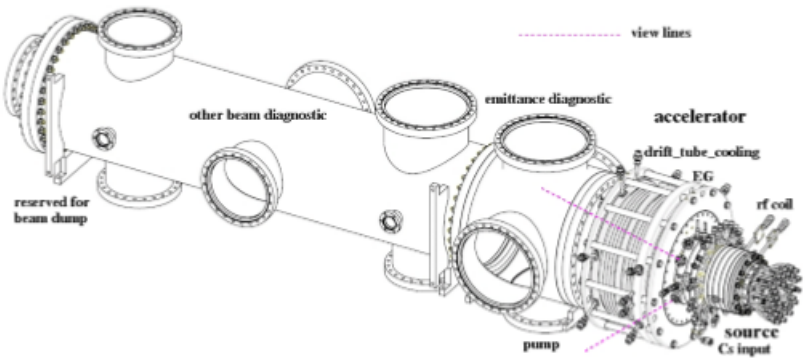

Figure 2: Nio1 ovrerall final version design

shown [7]. In figure 3 a section of NIO1 ion source is shown. [8]
According to figure 3, plasma in produced in the chamber (region 1 in the figure)

[3]Nation Institutes for Quantum and Radiological Science and Technology, Japan
[4]National Institute for Fusion Science, Japan
[5]Max-Planck-Institut fur Plasmaphysik, Germany
[6]Information about NIO1 were taken from [8] and [9]
[7]Picture 2 is taken from [9]
[8]Figure 3 is taken from [10]

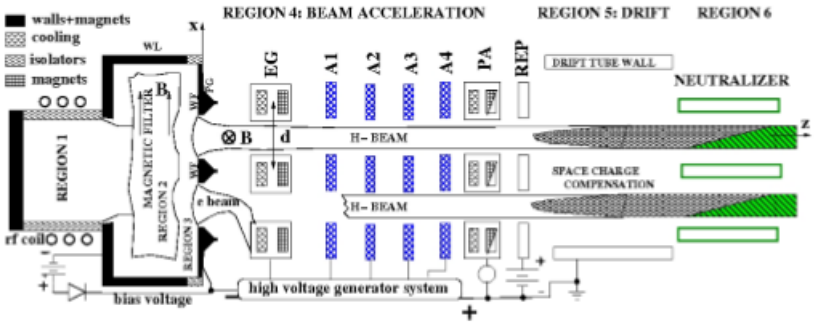

Figure 3: Longitudinal section (xz plane) of the NIO1 ion source and accelerator assembly.

by the series of coils shown in the figure. Then a magnetic filter (region 2) selects only negative hydrogen particles from the generated plasma; in region 3, where ions are collimated, electrons are discarted with a magnetic field thanks to they smaller Larmor radius. Negative ions are then accelerated, up to reach 60 keV kinetics energy (region 4), and injected in the neutralizer.
At first, the composition of NIO1 beam has to be clarified; the beam could be composed of nine, four or only one beamlet each one with a radius of 5 mm, a divergence of 5 mm/m and a nominal current of approximately 14.4 mA. In the nine and four beamlets set up, the beamlets are ordered in a 3x3 or 2x2 matrix; in those two configurations the distance beetwen two consecutive beamlets is 0.015 m.
In picture 4 an example of 3x3 beamlet configuration is shown. [9]
The final purpose of this thesis is making preliminary studies of the design of a

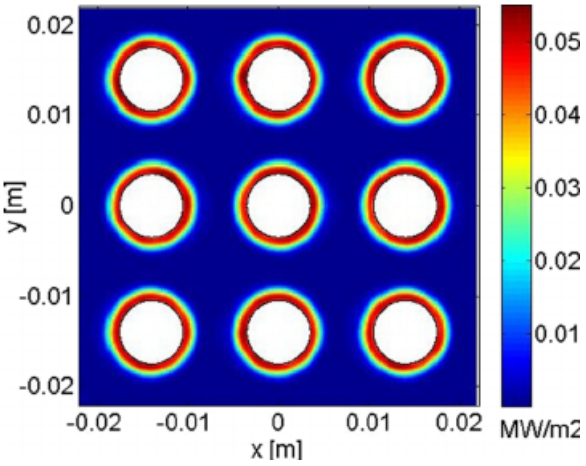

Figure 4: Longitudinal section (xy plane) of the NIO1 ion source

self powered plasma neutralizer for NIO1.
The actual NIO1 neutral gas neutralizer is a cylinder, a vessel with $R = 0.35$ m of radius and $L = 2$ m of length. NIO1 plasma neutralizer will be a smaller cylinder, coaxial to the vessel.
The model displayed in figure 5 shows the geometry form of the system, made of

[9] picture 4 is taken from [10]

two cylinders, that would compose NIO1 neutralizer.
Neutralizer form and characteristics will be extensively discussed in chapter 4. Neutral gas will be provided to the neutralizer by a pump at its center (represented by the down arrow), in order to mantain the chosen pressures P_1, P_2 and P_3 throughout the neutralizer-vessel system, while the vacuum in the vessel will be mantained by two cryogenic pumps (represented by the diagonal arrow).
The form of the neutralizer is chosen to keep a higher gas density along the path

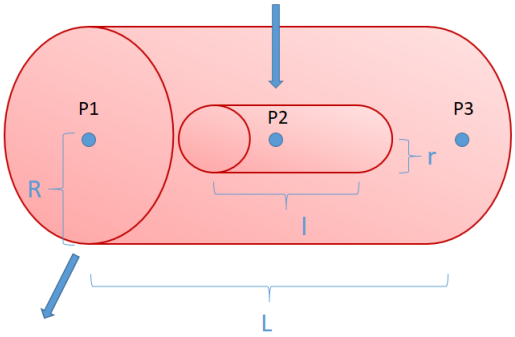

Figure 5: Neutralizer form

of the beam than in the other regions of the vessel, thus generating more plasma as described in sections 1.3.1 and 1.3.2.
It is assumed since the beginning that the length of the neutralizer, about one metre, will be much larger that its width, some centimetres, so all the plasma current generated in the neutralizer, will be assumed to be collected at its walls and not to be lost at the two ends of the neutralizer itself.

0.2 Thesis objectives

Firstly this thesis aims to extimate the neutralization efficiency of different degrees of ionization neutralizer.
The second objective is understanding why, in term of collisions, plasma neutralizers provide better efficiency than neutral gas ones.
Then the focus will move to NIO1 with the purpose of making preliminary studies for the design of a self powered plasma neutralizer for this experiment.
Great importance will be given to plasma confinement in order to reach the highest possible degree of ionization; then, an extimation of the efficiency of the proposed neutralizer models will be given.

Chapter 1

Particle beam evolution and plasma formation

The beam composition and its evolution along the neutralizer length were studied by a statistical model, which considers the most significant collisions of beam particles with the neutralizer target. The latter consists of a weakly ionized gas, composed by neutral hydrogen molecules or atoms, molecular and atomic ions and electrons.
Three H^- beam conditions were considered at three energies: 60 keV (NIO1), 200 keV (the energy of an experiment we will use to compare our predictions with experimental data [1], and which results are taken in [4]) and 1 MeV (ITER).
In the following, the beam-gas interactions (section 1.1) and their effects on a H^- beam (section 1.2) are discussed; later on, beam-induced effects on the gas are described (section 1.3) particularly considering the production of "slow" particles. Finally, the gas flow in molecular regime is described by a lumped model approach (section 1.4) to obtain the actual profile of gas density along the beam path.

1.1 Beam-gas interactions

Reactions affecting the charge state of the precursor negative ion beam are discussed in this section; to this purpose only the reactions which change the charge of the beam particles were considered.
Furthermore, in the relevant range, the impact energy of beam ions against gas particles at room temperature ($\simeq 0.03$ eV) is dominated by the beam energy, so kinetic energy in single collisions is the energy of the beam particle.
The collisional process listed in table 1.1 were considered. These include single and double ionization, responsible for primary ionization process, stripping, including all the precess analyzed in section 1.3.2, charge exchange, dissociation and others. Coolisional process can act on beam particles, or be a source of charges by gas ionization, thus generating a secondary plasma along the beam path. These two aspects are discussed in sections 1.2 and 1.3.

In table 1.1 simbols $\sigma^s_{ij} n_s$ follow the following convention: the subscripts i e j refer to the inizial and final charge states and the apexes e, i, g, h refer to reactions with electrons, ions, molecular gas and atomic hydrogen respectively.

[1] The experiment is located at the NBI Heating laboratory, Japan Atomic Energy Research Institute, 801-1 Mukoyama, Naka-machi, Naka-gun, Ibaraki-ken 311-0193, Japan

$H^- \rightarrow H^0$	σ_{60keV}	σ_{200keV}	σ_{1MeV}		simb.	ref
$H^-, H_2 \rightarrow H, H_2, e$	$5.44 \cdot 10^{-16}$	$2.53 \cdot 10^{-16}$	$4.94 \cdot 10^{-17}$	cm^2	σ^g_{-0}	[2] (p:F-8)
$H^-, H^+ \rightarrow H, H^+, e$	$2.92 \cdot 10^{-15}$	$2.00 \cdot 10^{-15}$	$8.00 \cdot 10^{-16}$	cm^2	σ^i_{-0}	[2] (p:F-6)
$H^+, H^- \rightarrow H, H$	$3.241 \cdot 10^{-16}$	$1.26 \cdot 10^{-16}$	$2.77 \cdot 10^{-17}$	cm^2	σ^i_{-0}	[2] (p:A-46)
$e, H^-[G] \rightarrow e, H[G], e, e$	$2.00 \cdot 10^{-18}$	$5.00 \cdot 10^{-19}$	$1.00 \cdot 10^{-19}$	cm^2	σ^e_{-0}	[11]
$H^-, H \rightarrow H, H, e$	$3.24 \cdot 10^{-16}$	$1.26 \cdot 10^{-16}$	$2.77 \cdot 10^{-17}$	cm^2	σ^h_{-0}	[2] (p:F-2)
$H^- \rightarrow H^+$	σ_{60keV}	σ_{200keV}	σ_{1MeV}		simb.	ref
$H^-, H_2 \rightarrow H^+, H_2, 2e$	$3.50 \cdot 10^{-17}$	$1.77 \cdot 10^{-17}$	$3.26 \cdot 10^{-18}$	cm^2	σ^g_{-+}	[2] (p:F-10)
$H^-, H \rightarrow H^+, H, 2e$	$1.03 \cdot 10^{-17}$	$3.53 \cdot 10^{-18}$	$8.00 \cdot 10^{-19}$	cm^2	σ^h_{-+}	[2] (p:F-4)
$H^+, H^- \rightarrow H^-, H^+$	$1.03 \cdot 10^{-17}$	$3.53 \cdot 10^{-18}$	$8.00 \cdot 10^{-19}$	cm^2	σ^i_{-+}	[2] (p:A-44)
$e, H^-[G] \rightarrow e, H^+, e, e$	$4.00 \cdot 10^{-19}$	$1.00 \cdot 10^{-19}$	$3.00.^{-20}$	cm^2	σ^e_{-+}	[11]
$H \rightarrow H^+$	σ_{60keV}	σ_{200keV}	σ_{1MeV}		simb.	ref
$H, H_2 \rightarrow H^+, H_2, e$	$1.19 \cdot 10^{-16}$	$7.4643 \cdot 10^{-17}$	$1.76 \cdot 10^{-17}$	cm^2	σ^g_{0+}	[2] (p:E-6)
$H, H_2 \rightarrow H^+, H^+, H^+, 3e$	$1.29 \cdot 10^{-18}$	$1.17 \cdot 10^{-18}$	$1.00 \cdot 10^{-18}$	cm^2	σ^g_{0+}	[2] (p:G-2)
$H, H_2 \rightarrow H^+, H, H^+, 2e$	$4.51 \cdot 10^{-19}$	$4.10 \cdot 10^{-19}$	$2.00 \cdot 10^{-19}$	cm^2	σ^g_{0+}	[2] (p:G-6)
$H, H \rightarrow H+, H, e$	$8.60 \cdot 10^{-17}$	$3.78 \cdot 10^{-17}$	$8.75 \cdot 10^{-18}$	cm^2	σ^h_{0+}	[2] (p:E-2)
$H^+, H[G] \rightarrow H^+, H^+, e$	$8.60 \cdot 10^{-17}$	$3.78 \cdot 10^{-17}$	$8.75 \cdot 10^{-18}$	cm^2	σ^i_{0+}	[11]
$H^+, H \rightarrow H, H^+$	$7.00 \cdot 10^{-17}$	$1.00 \cdot 10^{-18}$	$1.00 \cdot 10^{-19}$	cm^2	σ^h_{0+}	[11]
$e, H[1s] \rightarrow e, H^+, e$	$3.00 \cdot 10^{-19}$	$1.00 \cdot 10^{-19}$	$3.00 \cdot 10^{-20}$	cm^2	σ^e_{0+}	[12]
$H^+ \rightarrow H$	σ_{60keV}	σ_{200keV}	σ_{1MeV}		simb.	ref
$H^+, H[G] \rightarrow H[G], H^+$	$7.00 \cdot 10^{-17}$	$1.00 \cdot 10^{-18}$	$1.00 \cdot 10^{-19}$	cm^2	σ^h_{+0}	[11]
$H^+, H_2[G] \rightarrow H[G], H_2^+$	$7.00 \cdot 10^{-17}$	$1.00 \cdot 10^{-18}$	$4.00 \cdot 10^{-22}$	cm^2	σ^g_{+0}	[11]

Table 1.1: List of cross section of interation on beam particles with background gas

From figure 1.1 and table 1.1 it is clear that the most relevant reactions, for H^- beam fraction neutralisation, are: $H^-, H_2 \rightarrow H, H_2, e$ and $H^-, H^+ \rightarrow H, H^+, e$; while stripping and double stripping reactions $H, H_2 \rightarrow H^+, H_2, e$ and $H^-, H_2 \rightarrow H^+, H_2, 2e$ are the most relevant contributions to H^+ beam fraction. It is even shown that the most relevant reactions for each energy considered are the same. The cross sections of some reactions are not available at high energies, 200 keV and 1 MeV, but this mainly happens with minor reactions. For this reason they were approximated following the trend of reactions, whose cross sections where found, involving particles differing only by the sign of the charge. This is the case of single stripping on H^+ target: $H^-, H^+ \rightarrow H, H^+, e$ whose cross section was approximated at high energies by that of single stripping on H^0 target: $H^-, H \rightarrow H, H, e$.

1.2 Effects of the gas on the beam

The precursor negative ion beam will evolve by charge changing process occurring with the gas target. The neutral, positive and negative beam particles (Γ^0, Γ^+ and Γ^-) at a certain distance z from the accelerator are composed by H^0, H^+ and H^- respectively. They will evolve following the differential equation system 1.1 [2]

$$\begin{cases} \frac{d\Gamma^-}{dz} = \Gamma^+ \sum_s [\sigma^s_{+-} n_s] - \Gamma^- \sum_s [(\sigma^s_{-0} + \sigma^s_{-+}) n_s] + \Gamma^0 \sum_s [\sigma^s_{0-} n_s] \\ \frac{d\Gamma^0}{dz} = \Gamma^+ \sum_s [\sigma^s_{+0} n_s] + \Gamma^- \sum_s [\sigma^s_{-0} n_s] - \Gamma^0 \sum_s [(\sigma^s_{0+} + \sigma^s_{0-}) n_s] \\ \frac{d\Gamma^+}{dz} = -\Gamma^+ \sum_s [(\sigma^s_{+0} + \sigma^s_{+-}) n_s] + \Gamma^- \sum_s [\sigma^s_{-+} n_s] + \Gamma^0 \sum_s [\sigma^s_{0+} n_s] \end{cases} \quad (1.1)$$

[2] Equation 1.1 is taken from [5]

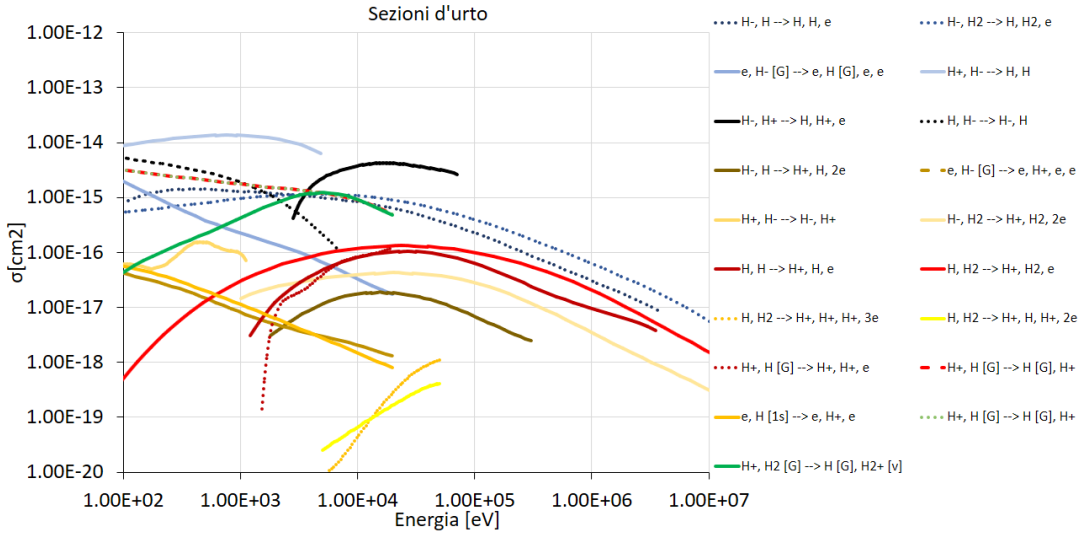

Figure 1.1: Cross section of interaction of beam particles with the gas target

In equation 1.1 summations and densities n ensue from 1.2.

$$\sum_s [\sigma^s_{ij} n_s] = \sigma^e_{ij} n_e + \sigma^i_{ij} n_i + \sigma^g_{ij} n_g + \sigma^h_{ij} n_h \tag{1.2}$$

System 1.1 is the general system to study the evolution of a beam, but, at the energy considered, cross sections relative to the production of H^- ions by beam particles can be neglected to semplify the system. According to 1.2 this semplification consists in assuming $\sum_s [\sigma^s_{+-} n_s] = \sum_s [\sigma^s_{0-} n_s] = 0$.
To solve the system an initial condition, describing the state of the beam immediately downstream the grounded grid of the electrostatic accelerator, is imposed:

$$\Gamma^-(0) = 1 \qquad \Gamma^+(0) = 0 \qquad \Gamma^0(0) = 0 \tag{1.3}$$

The new system will be:

$$\begin{cases} \frac{d\Gamma^-(z)}{dz} = -\Gamma^- \sum_s [(\sigma^s_{-0} + \sigma^s_{-+}) n_s] \\ \frac{d\Gamma^0(z)}{dz} = \Gamma^+ \sum_s [\sigma^s_{+0} n_s] + \Gamma^- \sum_s [\sigma^s_{-0} n_s] - \Gamma^0 \sum_s [\sigma^s_{0+} n_s] \\ \frac{d\Gamma^+(z)}{dz} = -\Gamma^+ \sum_s [\sigma^s_{+0} n_s] + \Gamma^- \sum_s [\sigma^s_{-+} n_s] + \Gamma^0 \sum_s [\sigma^s_{0+} n_s] \end{cases} \tag{1.4}$$

which, with the initial conditions 1.3, results integrable, results are shown in equation 1.5.
For example, figures 3.1, 3.2, 3.3 show the evolution of the three beam fractions

H^-, H^0, H^+ against target thickness which is simply defined at 3.2

$$\begin{cases} \Gamma^-(z) = exp((-\sigma^s_{-0}n_s - \sigma^s_{-+}n_s)\cdot z) \\ \Gamma^0(z) = -[-\sigma^s_{+0}n_s\sigma^s_{+0}n_s + \sigma^s_{+0}n_s\sigma^s_{-0}n_s - \sigma^s_{+0}n_s\sigma^s_{0+}n_s + \\ \quad +\sigma^s_{-0}n_s\sigma^s_{0+}n_s \cdot exp((-\sigma^s_{+0}n_s - \sigma^s_{0+}n_s)\cdot z) + \\ \quad +\sigma^s_{+0}n_s\sigma^s_{+0}n_s \cdot exp((-\sigma^s_{-0}n_s - \sigma^s_{-+}n_s)\cdot z) + \\ \quad -\sigma^s_{+0}n_s\sigma^s_{-0}n_s \cdot exp((-\sigma^s_{-0}n_s - \sigma^s_{-+}n_s)\cdot z) + \\ \quad +\sigma^s_{+0}n_s\sigma^s_{0+}n_s \cdot exp((-\sigma^s_{-0}n_s - \sigma^s_{-+}n_s)\cdot z) + \\ \quad -\sigma^s_{-0}n_s\sigma^s_{0+}n_s \cdot exp((-\sigma^s_{-0}n_s - \sigma^s_{-+}n_s)\cdot z) + \\ \quad +\sigma^s_{+0}n_s\sigma^s_{-+}n_s - \sigma^s_{+0}n_s\sigma^s_{-+}n_s \cdot exp((-\sigma^s_{+0}n_s - \sigma^s_{0+}n_s)\cdot z)]/ \\ \quad /[(\sigma^s_{+0}n_s + \sigma^s_{0+}n_s)(\sigma^s_{+0}n_s - \sigma^s_{-0}n_s + \sigma^s_{0+}n_s - \sigma^s_{-+}n_s)] \\ \Gamma^+(z) = -[-\sigma^s_{+0}n_s\sigma^s_{0+}n_s + \sigma^s_{-0}n_s\sigma^s_{0+}n_s - \sigma^s_{0+}n_s\sigma^s_{0+}n_s + \\ \quad +\sigma^s_{0+}n_s\sigma^s_{-+}n_s - \sigma^s_{-0}n_s\sigma^s_{0+}n_s \cdot exp((-\sigma^s_{+0}n_s - \sigma^s_{0+}n_s)\cdot z) + \\ \quad +\sigma^s_{+0}n_s\sigma^s_{0+}n_s exp((-\sigma^s_{-0}n_s - \sigma^s_{-+}n_s)\cdot z) + \\ \quad +\sigma^s_{0+}n_s\sigma^s_{0+}n_s \cdot exp((-\sigma^s_{-0}n_s - \sigma^s_{-+}n_s)\cdot z) + \\ \quad +\sigma^s_{+0}n_s\sigma^s_{-+}n_s \cdot exp((-\sigma^s_{+0}n_s - \sigma^s_{0+}n_s)\cdot z) + \\ \quad -\sigma^s_{+0}n_s\sigma^s_{-+}n_s \cdot exp((-\sigma^s_{-0}n_s - \sigma^s_{-+}n_s)\cdot z) + \\ \quad -\sigma^s_{0+}n_s\sigma^s_{-+}n_s \cdot exp((-\sigma^s_{-0}n_s - \sigma^s_{-+}n_s)\cdot z)]/ \\ \quad /[(\sigma^s_{+0}n_s + \sigma^s_{0+}n_s)(\sigma^s_{+0}n_s - \sigma^s_{-0}n_s + \sigma^s_{0+}n_s - \sigma^s_{-+}n_s)] \end{cases} \tag{1.5}$$

1.3 Beam effects on the gas

For the following studies it is also necessary to consider the effects of the beam on the backgroung gas which should provide the plasma required for a plasma neutralizer.

1.3.1 Beam induced ionization

If N is the local gas density, the charges I_{xb} generated per second in a neutralizer lenght Δz, by primary ionization by the beam particles, are given by:

$$I_{xb} = N I_{beam} \left[\Gamma^-\Sigma_{-x} + \Gamma^0\Sigma_{0x} + \Gamma^+\Sigma_{+x}\right]\Delta z \tag{1.6}$$

where $x = i, e$ refers to ions and electrons, while I_{beam}, A_n, and r are the beam *current*, the neutralizer $cross - section$ and the neutralizer *radius* respectively. Σ_{kx} represents the cross section for *slow* ion or electron production by the beam particles in the neutral gas so only ionization or similar are considered implying that $\Sigma_{ke} = \Sigma_{ki}$.

- $\Sigma_{-x} = 0\ cm^2$ see [3]

[3] Stripping is the only reaction of a H^- particles with a gas one that produces free electrons; anyway stripped electrons have higher energy than those produced by ionization and they have mainly the same direction as the primary beam, hence they have to be treated as a different plasma as will be seen in section 1.3.2

- $\Sigma_{0x} = \sigma_1 + \sigma_2 + \sigma_3 + 2\sigma_4 + 2\sigma_5 + \sigma_6 = 1.43^{-16}\ cm^2$ see [4]
- $\Sigma_{+x} = \sigma_7 = 2.06^{-16}\ cm^2$

with the cross sections σ_n $(n = 1, ..., 7)$ in table 1.2.
As we can see from table 1.2 the cross section of ionization of molecular hydrogen

reaction		σ	at	60 keV	[ref]
$H, H_2 \rightarrow H, H_2^+, e$	$\rightarrow$	σ_1	=	$1.35 \cdot 10^{-16}\ cm^2$	[2] p:D-4
$H, H_2 \rightarrow H^-, H^+, H^+, e$	$\rightarrow$	σ_2	=	$1.90 \cdot 10^{-19}\ cm^2$	[2] p:G-2
$H, H_2 \rightarrow H, H, H^+, e$	$\rightarrow$	σ_3	=	$1.00 \cdot 10^{-18}\ cm^2$	[2] p:G-4
$H, H_2 \rightarrow H, H^+, H^+, 2e$	$\rightarrow$	σ_4	=	$3.50 \cdot 10^{-18}\ cm^2$	[2] p:G-2
$H, H_2 \rightarrow H^+, H^+, H^+, 3e$	$\rightarrow$	σ_5	=	$1.10 \cdot 10^{-18}\ cm^2$	[2] p:G-2
$H, H_2 \rightarrow H^+, H, H^+, 2e$	$\rightarrow$	σ_6	=	$3.75 \cdot 10^{-19}\ cm^2$	[2] p:G-2
$H^+, H_2 \rightarrow H^+, e, H_2^+, e$	$\rightarrow$	σ_7	=	$2.05 \cdot 10^{-16}\ cm^2$	[2] p:D-16

Table 1.2: Cross sections for ionization of background gas by 60 keV beam particles

σ_1 is much bigger than those of ionization of atomic hydrogen (cross sections from σ_2 to σ_6) so plasma generated by ionization will be considered made made of H_2^+ ions.

1.3.2 Ionization by stripped electrons

Fast electrons are produced by single or double stripping of the H^- beam fraction or ionization of the H^0 fraction caused by impact on H_2 moleculas. Normally, it is assumed that stripping electrons are generated with the same velocity as the beam particles.
Stripping reactions considered in the present work, and the related cross sections for 60 keV beam, are shown in table 1.3
Stripped electron current generated in given interval Δz, in a uniform neutral

reaction		σ	at	60 keV	[ref]
$H^-, H_2 \rightarrow H, e, H_2$	$\rightarrow$	σ_{-0}	=	$5.50 \cdot 10^{-16}\ cm^2$	[2] p:F-8
$H^-, H_2 \rightarrow H^+, 2e, H_2$	$\rightarrow$	σ_{-+}	=	$3.50 \cdot 10^{-17}\ cm^2$	[2] p:F-10
$H^0, H_2 \rightarrow H^+, e, H_2$	$\rightarrow$	σ_{0+}	=	$1.18 \cdot 10^{-16}\ cm^2$	[2] p:E-6

Table 1.3: Cross sections of generation of stripping electrons by 60 keV beam particles on the background gas

gas, is given by:

$$I_s = \Gamma^- I_b \left[1 - e^{(-N(z)(\sigma_{-0} + 2\sigma_{-+})\Delta z)}\right] + \Gamma^0 I_b \left[1 - e^{(-N(z)\sigma_{0+}\Delta z)}\right] \tag{1.7}$$

[4] σ_4 and σ_5 are summed twice because they refer to double ionization reactions as shown in table 1.2

Discretizing the length of the neutralizer, the total stripped electron current generated at a given position $z_l = \sum_i^l \Delta z_i$ is given by:

$$I_{tots}(z_l) = \sum_i^l \left\{ \Gamma_i^- I_b \left[1 - e^{(-N_i(\sigma_{-0} + 2\sigma_{-+})\Delta z_i)} \right] + \Gamma_i^0 I_b \left[1 - e^{(-N_i \sigma_{0+} \Delta z_i)} \right] \right\} \tag{1.8}$$

The stripped electrons make up a third plasma with different characteristics than the other two considered: the beam and the primary ionization plasma. The energy of the stripped electrons would be $E_s = \frac{m_e}{m_b} E_b \simeq 33.3$ eV for a 60 keV Hydrogen beam.
The 33.3 eV stipped electrons could contribute to the plasma current by ionization of the background gas

$$I_{xs} = I_s N \Sigma_{sx} \frac{w_b}{2} \tag{1.9}$$

where Σ_{sx} is the cross section for ionization of the background gas by the stripped electrons given by

$$\Sigma_{sx} = \sigma_{sx1} + \sigma_{sx2} \tag{1.10}$$

In table 1.4 values for σ_{sx1} and σ_{sx2} are shown.

reaction		σ	for	33.3 eV	[ref]
$e, H_2[G] \rightarrow e, H_2^+, e$	$\rightarrow$	σ_{sx1}	=	$1.26 \cdot 10^{-16}\ cm^2$	[11]
$e, H_2[G] \rightarrow e, H^+, H[G], e$	$\rightarrow$	σ_{sx2}	=	$1.60 \cdot 10^{-18}\ cm^2$	[11]

Table 1.4: Cross sections of ionization by 33.3 eV stripped electrons

1.3.3 Space charge compensation

In order for an ion beam to propagate, it is necessary that the beam space charge is compensated for. It means that charges of opposite sign with respect to the beam ions are trapped in the potential well initially produced by the beam. Such charges, which are electrons in the case of positive ion beams or positive ions in the case of negative ion beams, are typically produced by the beam itself, by ionizing the background gas. The process follows a time scale $\tau_{scc} \simeq \frac{1}{n_{gas}\sigma_{iz}v_{beam}}$ where n_{gas} is the gas density, σ_{iz} is the ionization cross section and v_{beam} is the beam particle speed.
With this assumpion a higher density of electrons and H_2^+ ions in the center of the neutralizer is predicted, compensating the spatial charges; the border conditions will be discused in chapter 2.1.1, while, beetwen the low plasma density of the border and the higher density of the center, a diffusive model will be assumed.

1.3.4 Simplified beam plasma model

Whit assuming all the generated plasma to be collected at the neutralizer walls, the local plasma density current generated by primary ionization will be:

$$j_{xb} = \frac{N I_{beam}}{A_n} \left[\Gamma^- \Sigma_{-x} + \Gamma^0 \Sigma_{0x} + \Gamma^+ \Sigma_{+x} \right] \frac{r}{2} \tag{1.11}$$

where r is the neutralizer radius and A_n is the neutralizer surface.
The contribution to ionization, and therefore to the particle flux at walls, given by stripped electrons is calculated in equation 1.12 and 1.13. One should notice that electron induced ionization is only possible for electron energies higher than the ionization potential for H_2 which is 13.6eV; for comparison, stripped electrons in a 60keV beam have 33.3 eV energy as mentioned.
The contribution of the ionization by stripped electrons to the plasma flux to the wall of the neutralizer will be calculated in analogy with section 1.3.2. The stripped electrons generated over a length Δz will be calculated as:

$$j_s = \frac{\Gamma^- I_{beam}}{A_b}\left[1 - e^{(-N(\sigma_{-0}+2\sigma_{-+})\Delta z)}\right] + \frac{\Gamma^0 I_{beam}}{A_b}\left[1 - e^{(-N\sigma_{0+}\Delta z)}\right]. \quad (1.12)$$

The total flux of the generated stripped electron at a given point z_l will be:

$$j_{tots}(z_l) = \sum_i^l \left\{ \frac{\Gamma_i^- I_{beam}}{A_b}\left[1 - e^{(-N_i(\sigma_{-0}+2\sigma_{-+})\Delta z_i)}\right] + \frac{\Gamma_i^0 I_{beam}}{A_b}\left[1 - e^{(-N_i\sigma_{0+}\Delta z_i)}\right]\right\}. \quad (1.13)$$

This approximation holds as long as the mean free path for electron scattering λ_e is larger than the lenght scale of the system. Typically, the cross section for momentum transfer at 33 eV is $5 \cdot 10^{20}\ m^2$ and typical H_2 densities are around $5 \cdot 10^{18}\ m^{-3}$ thus yielding $\lambda_e \simeq 4m$. Thus the plasma flux of ionization by stripped electrons will be:

$$j_{xs} = j_s N \Sigma_{sx} \frac{w_b}{2}. \quad (1.14)$$

The total plasma flux to the wall of the neutralizer is given by

$$j_x = j_{xb} + j_{xs} \quad (1.15)$$

In this calculation secondary electrons generated by the primary ones, which may have enough energy to ionize the background gas, will not be considered.

1.3.5 Plasma losses

Plasma loss, inside the neutralizer, is due to recombination of electrons with H_2^+ ions. The number of plasma particles loss per unity of volume and time, L will be calculated as:

$$L = n_e K_{e-rec} n_{H_2^+} \quad (1.16)$$

where in the quasi neutrality approximation $n_e = n_{H_2^+} = n_p$.
K_{e-rec} is the rate of recomination of the electrons on ions; electron speed is distributed according to Maxwell-Boltzmann energy distribution, thus
$K_{e-rec} =< v_e \sigma_{rec} >_{MB}$

1.4 Dynamics of neutral gas

Gas flow in high vacuum is called "molecular flow" because viscosity is negligible and only single collisions beetwen molecules play a significant role. In high vacuum, free molecular flow regime is often attained, a regime in which only collisions with solid surfaces determine the flow parameters.

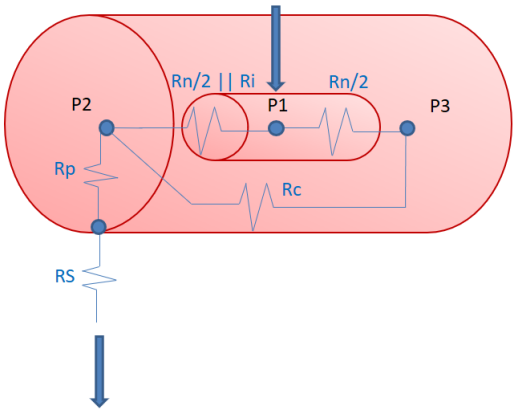

Figure 1.2: Resistive system canalisations in NIO1 neutralizer

In those conditions conductances through channels are indipendent from the pressure difference at the two sides of the channel, and the gas flux F is linearly dependent on the pressure difference:

$$F = C \cdot \Delta P \tag{1.17}$$

The resistence of a channel R will be the reciprocal of the conductance C; resistors in series will be summed like parallel conductances to realize a lumped model, such as in the electric circuits.
In this section conductances, for the system described in section 1.3 and shown in figure 5 are calculated.[5]
The resistive model for NIO1 neutralizer is shown in figure 1.2
Being D and d the diameters of the vessel and neutralizer, v_{rms} the root mean square of thermal speed of neutral gas at temperature T, L and l the lengths of the vessel and neutralizer, d_p and l_p the diameter and length of the tubes entering to the pumps, the following conductances are calculated.
The conductance entering the neutralizer from the vessel calculated as the conductance of a not small hole:

$$C_{en} = \frac{\pi v_{rms}}{4} \frac{\pi r^2}{1 - (\frac{d}{D})^2} \tag{1.18}$$

where r is the radius of the neutralizer.
The conductance for traversing half the length of the neutralizer (because gas is injected at the center of the neutralizer):

$$C_{tn/2} = \frac{\pi}{12} v_{rms} \frac{d^3}{l/2} \tag{1.19}$$

The conductance of traversing the cylindrical corona between the vessel and neutralizer:

$$C_{tc} = \frac{1}{3} \left(\frac{\pi RT}{2M} \right)^{\frac{1}{2}} \frac{(D-d)^2(D+d)}{l} K_f \tag{1.20}$$

where R is the gas constant, T the gas temperature and K_f a form factor that depends on the fraction d/D. In table 1.5 values of K_f against d/D are shown. To determine the value of K_f for each value of d/D those data were fit by a fourth

[5] All the statements and all the formulas about conductances in this section come from [13]

d/D	0	0.259	0.5	0.707	0.866	0.966
K_f	1	1.072	1.154	1.254	1.430	1.675

Table 1.5: Values of K_f

degree polynomial.
The conductance for entering the cylinndrical corona was calculated as the conductance for entering a hole with the diameter of the vessel minus the conductance for entering the neutralizer.

$$C_{ec} = \frac{1}{4} v_{rms} (A_{vessel} - A_{neutr}) \tag{1.21}$$

where A is the section of the vessel or of the neutralizer.
So the conductance of the circular corona will be calculated as:

$$C_c = \frac{C_{ec} \cdot C_{tc}}{C_{ec} + C_{tc}} \tag{1.22}$$

There is the conductance of the tube that goes from the vessel to the pump that consists in the conductance for entering a small tube:

$$C_{ep} = \frac{1}{4} v_{rms} \pi r_p^2 \tag{1.23}$$

and traversing the tube:

$$C_{tp} = \frac{\pi}{12} v_{rms} \frac{(2r_p)^3}{l_p} \tag{1.24}$$

So, similarly to equation 1.22 the total resistence of each tube will be:

$$C_p = \frac{C_{ep} \cdot C_{tp}}{C_{ep} + C_{tp}} \tag{1.25}$$

The last conductance in the considered system is the speed of the pumps C_s that completes the equivalent lumped model.
To extimate the time the experiment could stay on, before having to regenerate the pumps, is calculated as:

$$T = \frac{Q}{F_{tot}} \tag{1.26}$$

where Q is the total capacity of the pumps and F_{tot} it the total gas current.

Chapter 2

Plasma confinement

Two different possibilities were studied for the magnetic plasma confinement in the neutralizer in cylindrical geometry: the two possibilities are magnetic cusps and active coils. The former is made with permanent magnets around the neutralizer; the latter with an axial magnetic field produced by coils wound around the neutralizers so as to produce a magnetic mirror at both sides.
This chapter describes the two approaches and how to include these in the plasma loss terms.

2.1 Confinement with magnetic Cusps

This type of confinement involves the deployment of several permanent magnets with alternating poles, as shown in figure 2.1. Magnetic cusp are used to increase plasma density in the neutralizer by reducing the loss area and so changing the boundary conditions. [1]

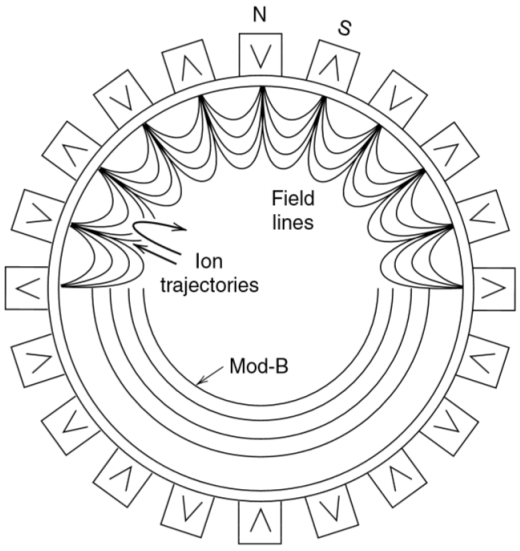

Figure 2.1: Section, in cylindrical coordinates, of magnetic cusp configuration.

[1] Immage 2.1 comes from [14]

2.1.1 Boundary conditions

The usual condition, for a $quasi - neutral$ plasma, $j_e = j_i$, in the considered system, considering the stripped electron, plasma and the charge exchange flux, is replaced by: [6]

$$j_i - \frac{j_e}{4} e^{(-\frac{\varphi}{T_e})} - j_s e^{(-\frac{\varphi}{E_{sB}})} = j_{cx} - j_s \tag{2.1}$$

where $j_{i,e}$ are defined in equation 1.15 (with the convention $x = i, e$), φ is the plasma potential, j_s is the stripped electron flux defined in equation 1.16, T_e is the electron temperature, E_{sB} is the energy of the stripped electron at the border (approximately 33 eV) and j_{cx} is the charge exchange flux. Equation 2.1 implicitly assumes that the charges generated at a given axial point z flow to the neutralizer walls at the same position z where they are generated. This is in general the case for a neutralizer tube having a small aspected ratio beetwen diameter and length: $d/l << 1$.
It is calculated the average number of collisions the stripped electrons have with the background gas along the neutralizer n_c, given by: [2]

$$n_c = \int_0^l n_{gas}(x)\sigma_{eH_2} dx \tag{2.2}$$

Calculating 2.2 for 33.3 eV electrons, a constant gas density, $n_{gas} = 1 \cdot 10^{19}\ m^{-3}$, for a beam path of length 1 m, it is obtained that almost a tenth of the stripped electrons will collide before being lost at the end of the neutralizer.
For this reason stripped electron will be treated as a untermalized beam with the same direction as the ion beam; therefore the stripped electron current at the walls of the neutralizer, j_s in equation 2.1, will be assumed equal to 0 A/m^2.
With this consideration equation 2.1 becomes:

$$0.6 n_i \left(\frac{eT_e}{m_i}\right)^{0.5} - \frac{n_e}{4}\left(\frac{8eT_e}{\pi m_e}\right)^{0.5} e^{(-\frac{\varphi}{T_e})} = \Psi n_i \left(\frac{eT_e}{m_i}\right)^{0.5} \tag{2.3}$$

where the factor 0.6 represents the drop of ion density at the plasma pre-sheath predicted in Bohm theory, and $\left(\frac{eT_e}{m_i}\right)^{0.5}$ is the ion sound speed, the speed of ions entering the Debay sheath. Lastly $\Psi = j_{cx}/j_x \simeq 0$, where j_x is the electron or ion current.
As $n_i = n_e = n_p$ at the plasma boundary, the plasma density is given by:

$$n_p = \frac{j_p}{e} \frac{1}{\left(\frac{eT_e}{m_i}\right)^{0.5}} \tag{2.4}$$

With the plasma density current j_p calculated in equation 1.15

2.1.2 Plasma density

The relevant quantity in plasma confinement is leak width w of a line of cusps. The leak width indicates the loss area of plasma to the walls. As shown in figure

[2] σ_{eH_2} is the sum of the cross sections of four collisions the stripped electrons could make with H_2 particles: dissociation ($\sigma_{dis} \simeq 1.58 \cdot 10^{-21} m^2$), ionization ($\sigma_{ion} \simeq 1.26 \cdot 10^{-20} m^2$), single dissociative ionization ($\sigma_{sdi} \simeq 1.60 \cdot 10^{-22} m^2$), and excitation ($\sigma_{exc} \simeq 3.66 \cdot 10^{-22} m^2$) [11]

2.1 magnetic cusp reduce the loss area.
If N is the number of cusps and w the leak width the effective loss circumference will be Nw. So the fraction of ions/electrons lost by ambipolar diffusion at the walls will be:

$$f_{loss} = \frac{Nw}{2\pi R} \qquad [14] \tag{2.5}$$

where R is the circumference of the neutralizer.
Total plasma current generated inside the neutralizer $I_x = I_{xb} + I_{xs}$ (calculated in equations 1.6 and 1.9) must be equal to the current collected to the walls of the neutralizer, considering that the whole plasma is lost at the walls.
This implies plasma current density to be $\frac{1}{f_{loss}}$ time bigger than without plasma confinement. Substituting in equation 2.4, plasma density in the neutralizer with magnetic cusp confinement will be obtained.

$$n_p = \frac{j_p}{f_{loss}} \frac{1}{e} \frac{1}{\left(\frac{eT_e}{m_i}\right)^{0.5}} \tag{2.6}$$

It is lastly observed that in this model recombination of electrons with H_2^+ ions in not considered, so 2.6 will probably overestimate n_p.
An extimation of the leak width, from theoretical calculation for low pressures, is given by Liebermann [14] [3]

$$w \simeq 4(r_{ce} r_{ci})^{0.5} \tag{2.7}$$

The geometric mean beetwen ion and electron Larmor radii: r_{ci} and r_{ce}.

2.2 Axial magnetic field

A second possiblity for plasma confinement is an axial magnetic field. The magnetic field, produced with a series of coils wound around the neutralizer, should give a larger confinement time to the plasma particles along its field lines, reducing the loss of plasma at the walls of the neutralizer. To reduce the loss at the two ends of the neutralizer, a magnetic mirror is produced increasing the number of windings at both sides.
In this case the steady state plasma density can be calculated by a diffusive model, that provides the plasma density in the volume by taking into account the different transport coefficients in a magnetic field. To this purpose, a 2D model was prepared to quantify plasma confined: all the currents, densities, all the quantities related with diffusion and transport and the magnetic field itself were calculated *point-by-point* in a grid representing the axial dimension $\hat{z}$ and the radial direction $\hat{r}$, with assuming a reasonable symmetry along the azimuthal coordinate θ. The radius of the netralizer will be divided into n_r intervals of length $\Delta r = R/n_r$, while its length will be divided into n_z intervals of length $\Delta z = L/n_z$.
Magnetic field was calculated in 3D space and then projected onto 2D. Magnetic field was calculated by a program that maps the magnetic field produced by a single coil iterated for the all coils, using the superposition principle.
In figure 2.2 and 2.3 an example of configuration of the magnetic field is shown; it is produced by a 100 coils, wound along the neutralizer, each one with a radius of

[3] In [14] Liebermann cites Hershkowitz et al., 1975

0.045 m and a current of 1000 A. In this simulation magnetic field was calculated only inside the neutralizer (of 0.04 m of radius, 1.30 m of length and positioned 0.40 m far from the beginning of the vessel) and in the two zones, before and after the neutralizer, that are within 0.04 m from the axis of the neutralizer. The magnetic mirror is obtained thanks to five coils all wound at the begining and at the end of the neutralizer.
As shown in figures 2.2 and 2.3, in the majority of the volume of the neutralizer, the axial component of the magnetic fiel, B_z, is dominant on the radial one, B_r. This consideration will be significant in section 2.2.1.

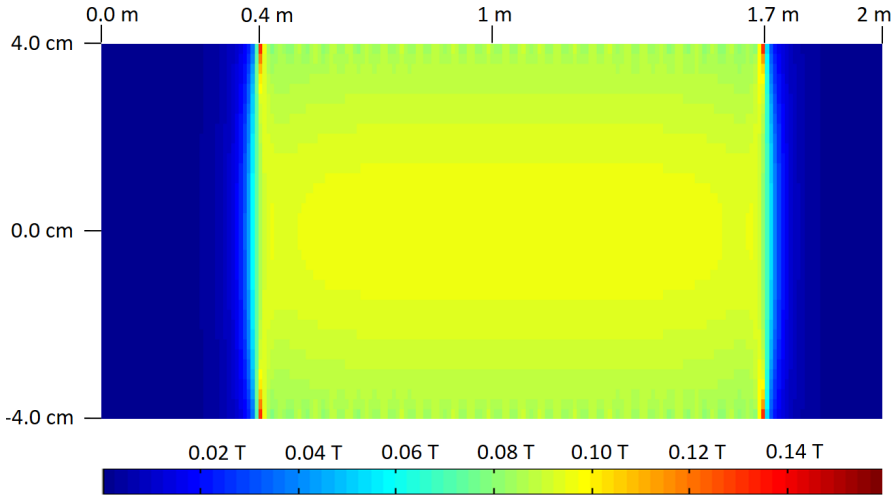

Figure 2.2: Axial component of the magnetic field: B_z, before, inside and after the neutralizer

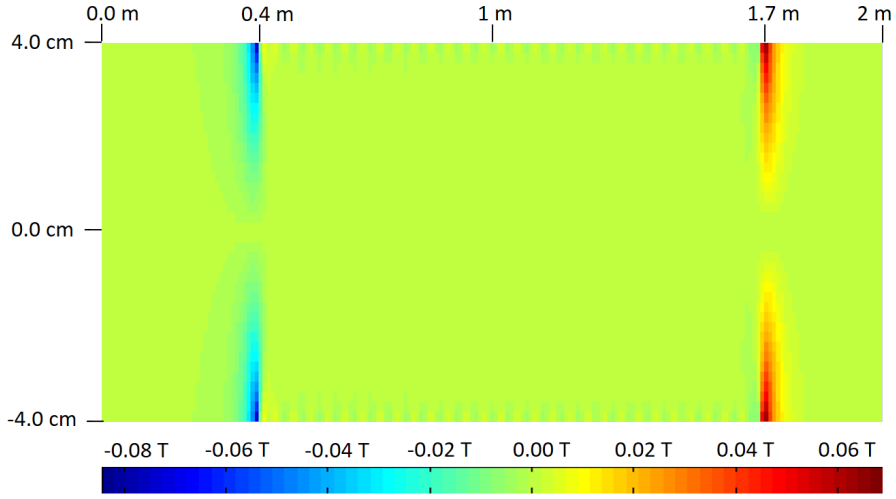

Figure 2.3: Radial component of the magnetic field: B_r, before, inside and after the neutralizer

2.2.1 Charged particle dynamics

Plasma dynamics will be determined by four forces: the pressure gradient, the collisions beetwen particles, the Lorentz force, and the force due to the gradient of the magnetic field.
The motion equation for each species: H_2^+ ions and electrons will be [4]:

$$0 = qn_p(\boldsymbol{E} + \boldsymbol{u} \times \boldsymbol{B}) - n_p|\boldsymbol{m}_x|\boldsymbol{\nabla}|B| - kT_x\boldsymbol{\nabla}n_p - m_x n_x \nu_{mx}\boldsymbol{u} \tag{2.8}$$

where $x = i, e$ refers to ions and electrons, n_p is the plasma density, equal for both species, $\boldsymbol{m}$ is the magnetic moment, m is the mass and ν_m is the momentum transfer elastic collision frequency. The following system will be obtained for ions and electrons:

$$\begin{cases} 0 = qn_pE_z + qn_x(u_r^x B_\theta - u_\theta^x B_r) - n_p|\boldsymbol{m}_x|\nabla_z|B| - kT_x\frac{\partial n_p}{\partial z} - m_x n_p \nu_m^x u_z^x \\ 0 = qn_pE_\theta + qn_x(u_z^x B_r - u_r^x B_z) - n_p|\boldsymbol{m}_x|\nabla_\theta|B| - kT_x\frac{\partial n_p}{\partial \theta} - m_x n_p \nu_m^x u_\theta^x \\ 0 = qn_pE_r + qn_x(u_\theta^x B_z - u_z^x B_\theta) - n_p|\boldsymbol{m}_x|\nabla_r|B| - kT_x\frac{\partial n_p}{\partial r} - m_x n_p \nu_m^x u_r^x \end{cases} \tag{2.9}$$

whith the usual convention $x = e, i$ To simplify the two systems, vectors $\boldsymbol{B}$ and $\boldsymbol{\nabla}|B|$ will be further assumed to be parallel to the axis of the neutralizer throughout the neutralizer itself. This is not a very physical assumption because it would violate the law $\nabla \cdot \boldsymbol{B} = 0$. Anyway, it greatly semplifies equation 2.9 without loosing much information for the two following reasons: the first is that the length of the neutralizer will be much bigger than its diameter, implying the magnetic field, in this configuration, to be constant and parallel to $\hat{z}$ for the majority of the volume of the neutralizer, as as it was shown in the previous simulation. The second reason is that the two regions, where the magnetic field $\boldsymbol{B}$ is not parallel to $\hat{z}$, the two ends of the neutralizer, are not so relevant for gas ionization and plasma confinement: that is because in the initial part the beam radius is smaller, so the ionization is concentrated closely to the axis where the magnetic field is parallel to $\hat{z}$; while the plasma generated by ionization in the ending region will be mainly lost following the magnetic lines out of the neutralizer. Ratio $\frac{|B_r|}{|B_z|}$ is shown in figure 2.4
In figure 2.4 the two black lines indicate the two ends of the neutralizer; as shown in the figure, inside the neutralizer, assuming $\boldsymbol{B} \parallel \hat{z}$ is not that far from reality. This semplification makes the plasma flux perpendicular to $\boldsymbol{B}$ ($\boldsymbol{\Gamma}_\perp$), to be indipendent from magnetic field gradient, so the dynamics will be determined by the usual ambipolar perpendicular diffusion:

$$\Gamma_\perp = -D_{a\perp}\nabla_\perp n \tag{2.10}$$

so, assuming $\boldsymbol{B} \parallel \hat{z}$, the radial flux in cilindrical coordinates will be

$$\Gamma_r = -D_{a\perp}\frac{1}{r}\frac{\partial(rn)}{\partial r} \tag{2.11}$$

Along the axis of the neutralizer, with the previous simplification and upon solving for u_z^x, equation 2.9 becomes:

$$u_z^x = \mu^x E_z - \frac{|\boldsymbol{m}_x|}{m_x \nu_m^x}\frac{\partial B}{\partial z} - D_x\frac{1}{n_p}\frac{\partial n_p}{\partial z} \tag{2.12}$$

[4] equation 2.8 comes from [15]

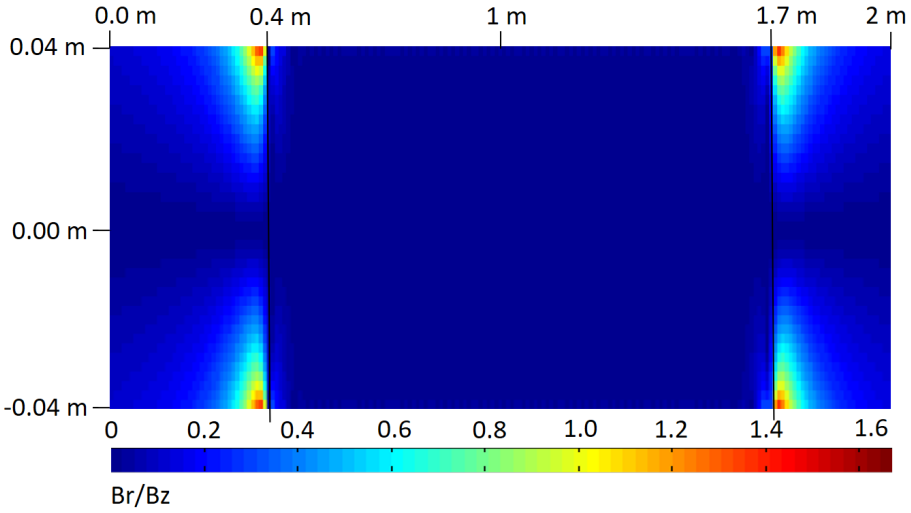

Figure 2.4: Ratio $\frac{|B_r|}{|B_z|}$

Where $\mu_x = \frac{q}{m_x \nu_m^x}$ and $D_x = \frac{KT_x}{m_x \nu_m^x}$ are the mobility and diffusive coefficient of the *x-species*.
Imposing $u_z^i = u_z^e$ and carring out E_z it is obtained:

$$E_z = \frac{\nabla_z B}{\mu_i + \mu_e}\left(\frac{|\boldsymbol{m}_i|}{m_i \nu_m^i} - \frac{|\boldsymbol{m}_e|}{m_e \nu_m^e}\right) + \frac{1}{n_p}\frac{\partial n_p}{\partial z}\left(\frac{D_i - D_e}{\mu_i + \mu_e}\right) \tag{2.13}$$

By substituting equation 2.13 in equation 2.12 for ions or elecrons, upon solving for the plasma current along $\hat{z}$: $\Gamma_z = n_p u_z$, it is obtained:

$$\Gamma_z = -D_a \frac{\partial n_p}{\partial z} - n_p \nabla_z B\left(\frac{\mu_i N_e + \mu_e N_i}{\mu_i + \mu_e}\right) \tag{2.14}$$

where $D_a = \frac{\mu_i D_e + \mu_e D_i}{\mu_i + \mu_e}$ is the ambipolar diffusive coefficient, and $N_x = \frac{|\boldsymbol{m}_x|}{m_x \nu_m^x}$ is a coefficient related to a single species. To simplify the equation further $N_a = \frac{\mu_i N_e + \mu_e N_i}{\mu_i + \mu_e}$ was introduced similarly to D_a.
After those calculations the plasma flux $\boldsymbol{\Gamma}$ in the $2D - model$ was obtained:

$$\boldsymbol{\Gamma} = \begin{cases} -D_a \frac{\partial n_p}{\partial z} - n_p(\nabla_z B) N_a & \hat{z}, \\ -D_{a\perp} \frac{\partial n_p}{\partial r} & \hat{r}. \end{cases} \tag{2.15}$$

2.2.2 Plasma density

It was further imposed the conservation of the electric charge in cylindrical coordinates:

$$\boldsymbol{\nabla} \cdot \boldsymbol{\Gamma} = \frac{\partial \Gamma_z}{\partial_z} + \frac{1}{r}\frac{\partial (r\Gamma_r)}{\partial r} = G - L \tag{2.16}$$

where G and L are plasma generation and loss.
The source term, G, can be calculated as

$$G = j_{ion} n_y \sigma_y^i \tag{2.17}$$

where j_{ion} is the ionising current (beam current or stripped electron current as widely described in section 1.3), n_y is the density of the target y (that refers to

neutral gas or plasma) and σ_y^i is the cross section of ionization of the species y by the ionising particle.[5]
Plasma loss (L) in the neutralizer, in this model, will be given by recombination of thermal electrons with H_2^+ ions. Ions will be considered fixed and the electron speed to be distributed according to a Maxwell-Boltman distribution of temperature T_e; the loss term will be calculated as:

$$L = n_e K_{rec} n_i \tag{2.18}$$

where $K =< \sigma_{rec} v_e >_{MB}$ is the rate coefficient of recombination: the average of the cross section of recombination σ_{rec} ([11]) times the electron speed integrated over the Maxwell-Boltzmann distribution of the electrons.
Equation 2.16 turns into the partial differential equation 2.19; upon solving this equation, for each point of our 2D grid, the plasma density will be found.

$$\begin{aligned}[\boldsymbol{\nabla}\cdot\boldsymbol{\Gamma}]_{r_i,z_k} = \left[-\frac{\partial D_a}{\partial z}\frac{\partial n_p}{\partial z} - D_a\frac{\partial^2 n_p}{\partial z^2} - \frac{\partial n_p}{\partial z}\frac{\partial B}{\partial z}N_a - n_p\frac{\partial^2 B}{\partial z^2}N_- n_p\frac{\partial B}{\partial z}\frac{\partial N_a}{\partial z}\right]_{r_i,z_k} + \\ - \left[\frac{1}{r}D_{a\perp}\frac{\partial n_p}{\partial r} - \frac{\partial D_{a\perp}}{\partial r}\frac{\partial n_p}{\partial r} - D_{a\perp}\frac{\partial^2 n_p}{\partial r^2}\right]_{r_i,z_k} = [G-L]_{r_i,z_k}\end{aligned} \tag{2.19}$$

where $r_i = i\cdot\Delta r$ and $z_k = k\cdot\Delta z$ with $i = 1,...,n_r$ and $k = 1,...,n_z$ refers to the points of the grid.
Equation 2.19 is solved in the 2D symmetric domain with a relaxation method using the following formulas for the derivative calculation of the quantity $x(r,z)$:

$$\begin{aligned}\frac{\partial x(r,z)}{\partial r}|_{i,k} &= \frac{x_{i+1,k} - x_{i-1,k}}{2\Delta r} \\ \frac{\partial x(r,z)}{\partial z}|_{i,k} &= \frac{x_{i,k+1} - x_{i,k-1}}{2\Delta z}\end{aligned} \tag{2.20}$$

and

$$\begin{aligned}\frac{\partial^2 x(r,z)}{\partial r^2}|_{i,k} &= \frac{x_{i+1,k} + x_{i-1,k} - 2x_{i,k}}{\Delta r^2} \\ \frac{\partial^2 x(r,z)}{\partial z^2}|_{i,k} &= \frac{x_{i,k+1} + x_{i,k-1} - 2x_{i,k}}{\Delta z^2}\end{aligned} \tag{2.21}$$

By substituting 2.20 and 2.21 for plasma density in equation 2.19 and upon solving for the plasma density calculated at a given point (i,k):

$$n_{i,k} = \frac{1}{A_{i,k}}\left(G_{i,k} - L_{i,k} + n_{i,j+1}B_{i,k} + n_{i,j-1}C_{i,k} + n_{i+1,j}D_{i,k} + n_{i-1,j}E_{i,k}\right) \tag{2.22}$$

[5] All the cross sections σ_y^i are in chapter 1.3

where $A_{i,k}$, $B_{i,k}$, $C_{i,k}$, $D_{i,k}$ and $E_{i,k}$ are coefficients whose expression is as follows:

$$\begin{aligned}
A_{i,k} &= \frac{\partial^2 B_z}{\partial z^2} N_a|_{i,k} + \frac{\partial B_z}{\partial z}\frac{\partial N_a}{\partial z}|_{i,k} + 2\frac{D_a}{\Delta z^2}|_{i,k} + \frac{2D_{a\perp}}{\Delta r^2}|_{i,k} \\
B_{i,k} &= \frac{D_a}{\Delta z^2}|_{i,k} + \frac{1}{2\Delta z}\left(\frac{\partial D_a}{\partial z} + \frac{\partial B_z}{\partial z}N_a\right)|_{i,k} \\
C_{i,k} &= \frac{D_a}{\Delta z^2}|_{i,k} - \frac{1}{2\Delta z}\left(\frac{\partial D_a}{\partial z} + \frac{\partial B_z}{\partial z}N_a\right)|_{i,k} \\
D_{i,k} &= \frac{D_{a\perp}}{\Delta r^2}|_{i,k} + \frac{1}{2\Delta r}\left(\frac{D_{a\perp}}{r} + \frac{\partial D_{a\perp}}{\partial r}\right)|_{i,k} \\
E_{i,k} &= \frac{D_{a\perp}}{\Delta r^2}|_{i,k} - \frac{1}{2\Delta r}\left(\frac{D_{a\perp}}{r} + \frac{\partial D_{a\perp}}{\partial r}\right)|_{i,k}
\end{aligned} \tag{2.23}$$

All the derivatives in equation 2.23 according to 2.20 and 2.21.

Chapter 3

Evolution of the beam through the neutralizer in different configurations

This chapter will treat the composition of three H^- beams through H_2 gas, with different degrees of ionization. The beam considered will be those three described in the introdution of chapter 1.
The objective of this chapter is to analyze the expected performances of a plasma neutralizer and, comparing with a gas cell neutralizer, to understand which are the neutralizing collisions, of beam particle with plasma, that ensure a plasma neutralizer better performances.

3.1 Beam composition

To simulate the evolution of the beam through the neutralizer equation 1.4 was used, with the initial conditions 1.3.
The evolution of the beams was studied through: neutral hydrogen gas, 10% and 30% degree of ionization hydrogen plasma; those percentage values were chosen to compare the obtained results with experimental data [4].
The ionization degree is defined as:

$$\chi = \frac{n_p}{n} \tag{3.1}$$

where n_p is the plasma density ans n is the total particle density: $n = n_{gas}+n_i+n_h$.
With this definition of plasma density it is assumed that in the secondary beam plasma, $quasi - neutrality$ is ensured: $n_e \simeq n_i \simeq n_p$.
In the next simulations the focus will be on knowing which is the composition of the beams after a certain target thickness $t.t.$ (defined in equation 3.2). The axial position z where a certain target thickness is reached is not considered in this section, pressures infact will be adapted to reach the chosen target thickness.

$$t.t.(l) = \int_0^l n(x)dx \tag{3.2}$$

With Knowing that the evolution of a beam in a gas follows equation 1.5, and with the cross section shown in table 1.1, for a 60 keV beam, the following results

are obtained shown in figures 3.1, 3.2 and 3.3.

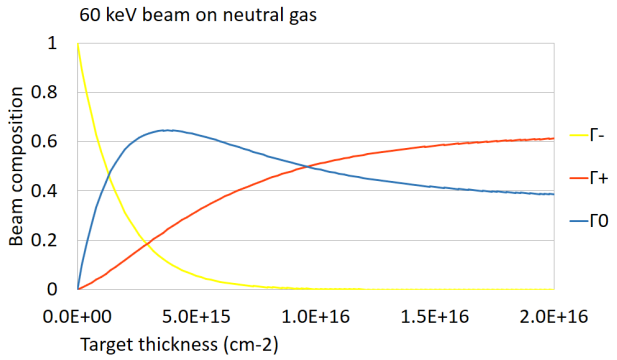

Figure 3.1: Composition of a 60 keV beam through neutral gas

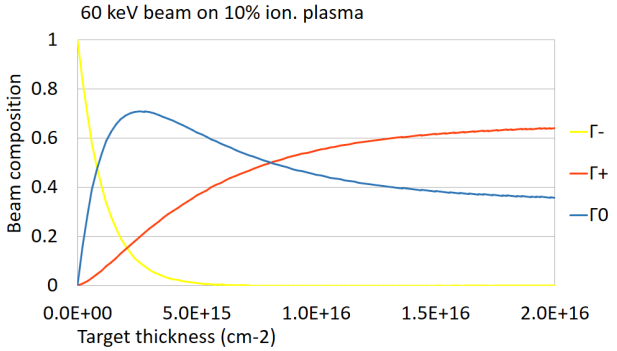

Figure 3.2: Composition of a 60 keV beam through 10% degree of ionization plasma

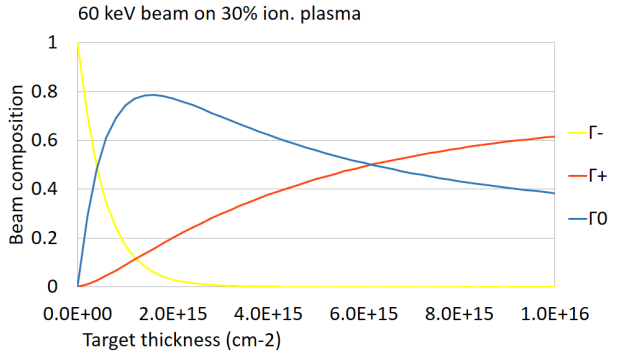

Figure 3.3: Composition of a 60 keV beam through 30% degree of ionization plasma

Evolution of a 200 keV beam was predicted in the same way, it is shown in figures 3.4, 3.5 and 3.6; and of a 1 MeV beam, results are shown in figures 3.7, 3.8 and 3.9.

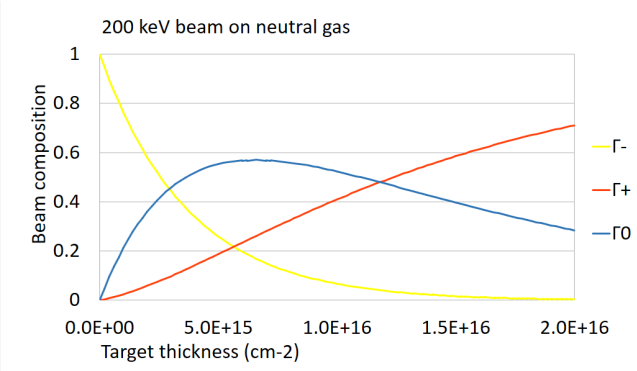

Figure 3.4: Composition of a 200 keV beam through neutral gas

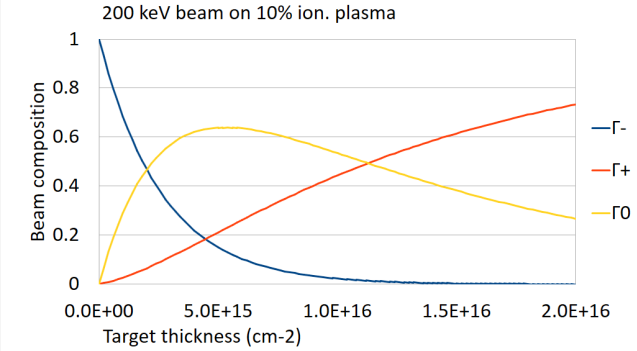

Figure 3.5: Composition of a 200 keV beam through 10% degree of ionization plasma

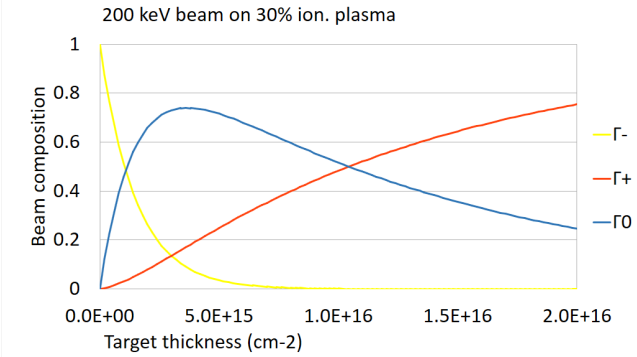

Figure 3.6: Composition of a 200 keV beam through 30% degree of ionization plasma

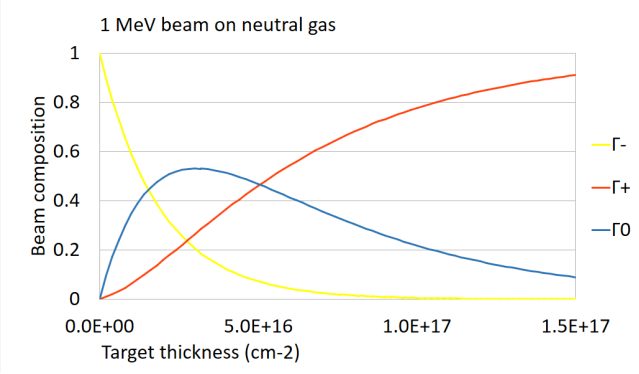

Figure 3.7: Composition of a 1 MeV beam through neutral gas

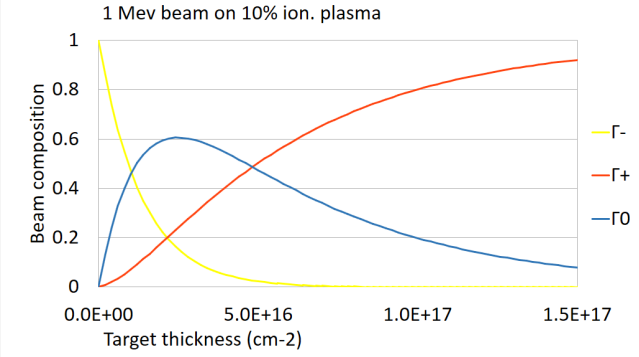

Figure 3.8: Composition of a 1 MeV beam through 10% degree of ionization plasma

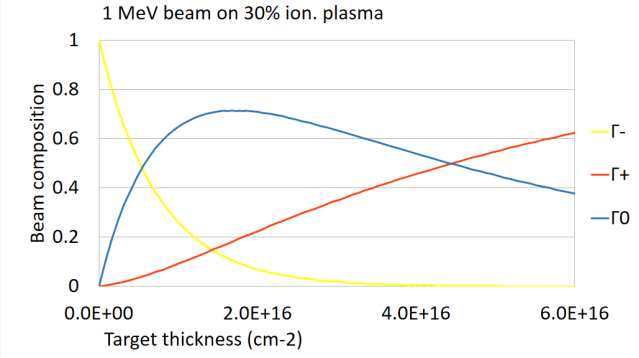

Figure 3.9: Composition of a 1 MeV beam through 30% degree of ionization plasma

In the figures, Γ^0 represents the efficiency of a neutralizer with a given target thickness and a given degree of ionization.
In the graphs it is shown that the target thickness at the point where $\Gamma^- = \Gamma^+$ is almost the target thickness when selecting the maximum of efficiency. This happens for all beam energies and for all degrees of ionization considered.
This is an advantageous coincidence, because, when selecting to work with the target thickness that optimizes neutralisation, also the same power at the and of the neutralizer is lost, in terms of H^- and H^+ particles.
For these two reasons during operation the total target thickness, at the end of the neutralizer is the one at the maximum of Γ^0.
Only two differences between the compositions of different energy beams are observed: the first is that, with increasing beam energy, a bigger target thickness is needed in order to optimize the efficiency; this is an obvious consequence of the fact that the cross sections are decreasing with increasing energy. The second difference is that upon increasing the beam energy the asymptotic value of Γ^0 decreases, but this is not a real problem because a neutralizer works in the first area of the graph, before the maximum of efficiency.
In figure 3.10, 3.11 and 3.12 the estimated efficiency of the 60 keV, 200 keV and 1 MeV beams, for neutralizers with different degrees of ionization, is shown against target thickness,.

The most important thing that figures 3.10, 3.11 and 3.12 show is that efficiency

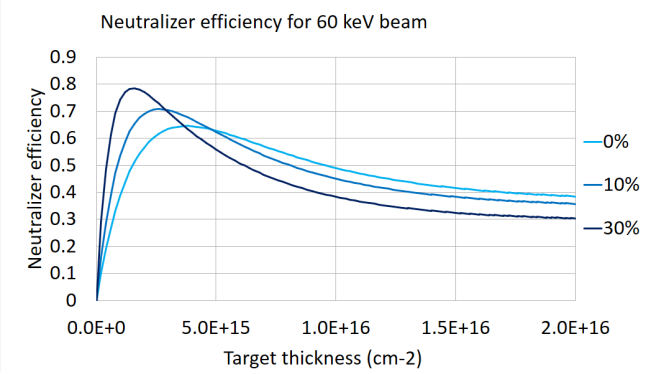

Figure 3.10: Efficiency of a 60 keV beam

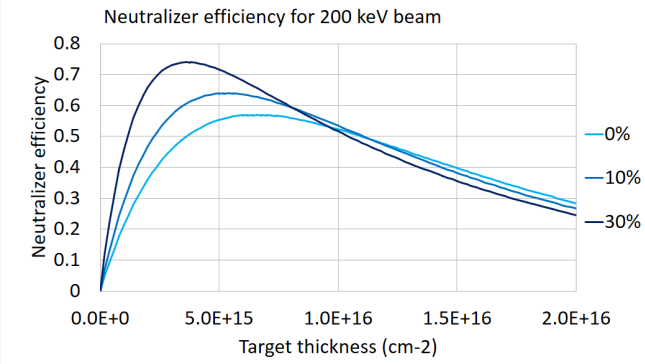

Figure 3.11: Efficiency of a 200 keV beam

increases with increasing plasma ionization degree, and it is also shown that it

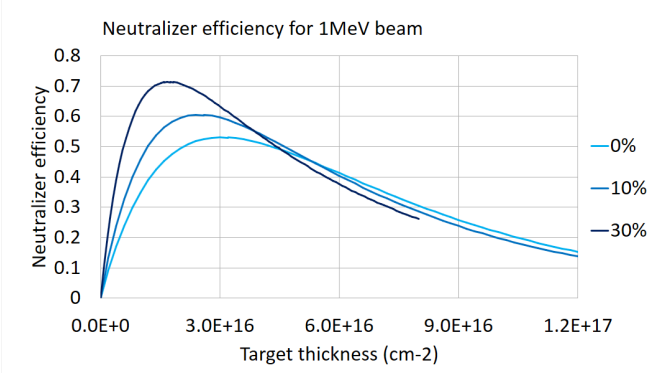

Figure 3.12: Efficiency of a 1 MeV beam

happens for all the energies considered. The higher the ionization degree, the higher the efficiency. Here it is confirmed that, in order to reduce the beam power loss in neutralisation a plasma neutralizer is needed; a plasma neutralizer infact could raise the performancees of neutral beam injector even more than ten percentage points.
In table 3.1 the maximum efficency estimed, for all considered configurations, is reported.
For NIO1 beam it is estimed the efficiency for a 10% degree of ionization to be

energy	$\chi = 0\%$	$\chi = 10\%$	$\chi = 30\%$
60keV	0.65	0.72	0.78
200 keV	0.57	0.64	0.74
1 MeV	0.54	0.61	0.72

Table 3.1: Expected efficiencies

almost ten percentage points higher than with a neutral one; the same happends for a 200 keV beam and for ITER beam.
In figures 3.10, 3.11 and 3.12 it is shown that the target thickness relative to the maximum of the efficiency decreases with increasing ionization degree. This can be a second advantage of the plasma neutralizer with respect to the neutral gas one: because a lower target thickness is provided by a lower gas density; the lower the gas density the longer the experiment could be kept on, according to equation 1.26.

energy	$\chi = 0\%$	$\chi = 10\%$	$\chi = 30\%$	
60 keV	$4 \cdot 10^{19}$	$3 \cdot 10^{19}$	$2 \cdot 10^{19}$	m^{-2}
200 keV	$7 \cdot 10^{19}$	$5 \cdot 10^{19}$	$4 \cdot 10^{19}$	m^{-2}
1 MeV	$3 \cdot 10^{20}$	$2.5 \cdot 10^{20}$	$1.5 \cdot 10^{20}$	m^{-2}

Table 3.2: Target thickness relative to the optimal efficiency

3.2 Relation with experimental data

As anticipated in capter 2, it was chosen to study the composition af a 200 keV beam to compare predictions with experimental data taken from [4].
Figure 3.13 shows a good agreement between experimental data and predicted efficiency.

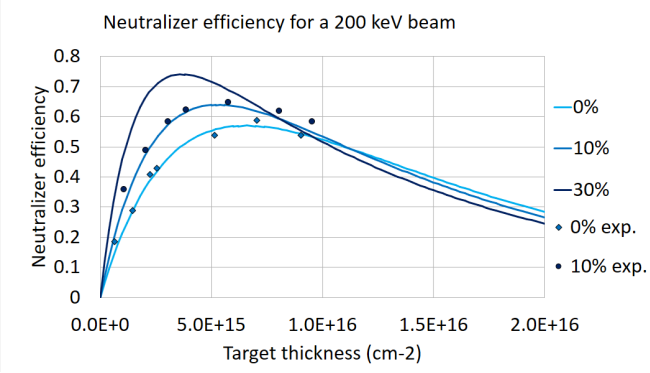

Figure 3.13: Estimation and eperimental data for efficiency of a 200 keV beam

3.3 Individuation of neutralizing collisions

In section 3.1 it was established that a plasma neutralizer ensures higher efficiencies that a neutral gas one. This section will treat, in two different ways, which type of collision guarantees the plasma neutralizer better efficiency than a neutral gas neutralizer.
In figure 3.14 the product $\sigma^s_{-0} n_s$ (s=g, e, i,h) is shown, that, according to the convention established in section 1.1, is the product of neutralisation cross section of H^- beam particles times the density of particles.
In the figure neutralizing collisions with neutral gas are in blue, while neutralizing collisions with plasma particles are in pink or similar colors.
With the same conventions, in figure 3.15 $\sigma^s_{0+} n_s$ (s=g, e,i,h), that represents the loss of H^0 beam particles by reionization, is shown.
In figures 3.14 and 3.15 it was chosen to calculate this quantity for a 30% degree of ionization plasma.
As it is shown in figure 3.14 the reaction $H^-, H^+ \rightarrow H, H^+, e$ makes the plasma contribution to neutralization about three times bigger than neutral gas, even if plasma density is less than half the neutral density; this happens for all considered energies.
In figure 3.15 it is shown that re-ionization given by collision with plasma particles is comparable to that with neutral gas; furthermore the neutralization term is about one order of magnitude higher than the re-ionization one.
The combination of these facts allows the plasma neutralizer to attain a better efficiency that a neutral gas one, for all energies considered.
A second way to study the contribution of plasma and neutral gas to neutralization involves studing the different contibutions, positive and negative, to the first derivative of the function Γ^0.

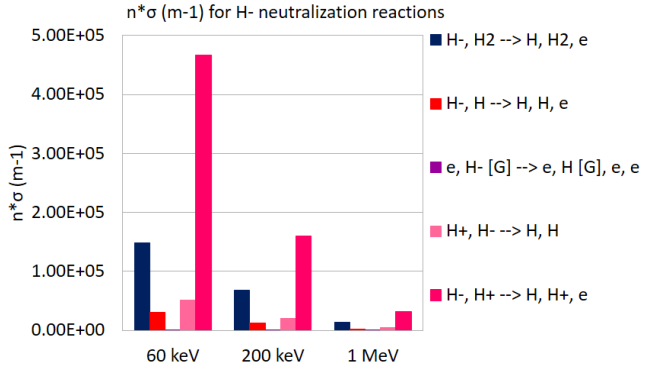

Figure 3.14: Evaluation of neutralizing collisions for a 30% degree of ionization plasma

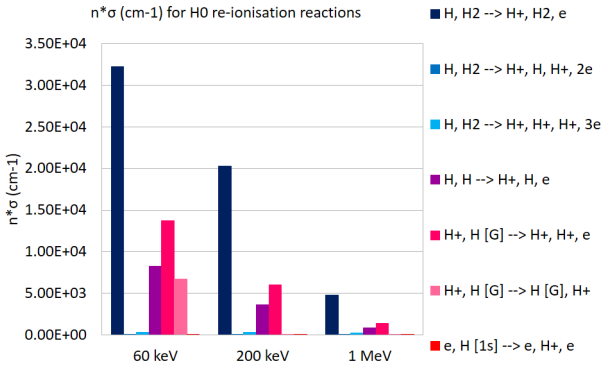

Figure 3.15: Evaluation of re-ionizing collisions for a 30% degree of ionization plasma

From equation 1.4:

$$\frac{d\Gamma^0(z)}{dz} = \Gamma^+(z)\sum_s[\sigma^s_{+0}n_s] + \Gamma^-(z)\sum_s[\sigma^s_{-0}n_s] - \Gamma^0(z)\sum_s[\sigma^s_{0+}n_s] \tag{3.3}$$

splitting the neutral gas and plasma contribution it is obtained:

$$\begin{cases} \frac{d\Gamma^0(z)}{dz} = \Gamma^+(z)\left(\sigma^g_{+0}n_g + \sum_x[\sigma^x_{+0}n_x]\right) + \Gamma^-(z)\left(\sigma^g_{-0}n_g + \sum_x[\sigma^x_{-0}n_x]\right) + \\ \quad -\Gamma^0(z)\left(\sigma^s_{0+}n_s + \sum_x[\sigma^x_{0+}n_x]\right) \end{cases} \tag{3.4}$$

where $x = i, e, h$.
In figure 3.16, 3.17 and 3.18 the cumulative graphs are shown for positive and negative contribution to the first derivative of Γ^0 for a 60 keV beam at the usual degrees of ionization.

Obviously in figure 3.16 the contribution of reactions with the plasma is zero throughout all the target thickness crossed by the beam. In figure 3.17 but even more in 3.18 it is shown that the plasma positive contribution to the first derivative is much higher than its negative contribution.
Comparing figure 3.16 with 3.18 is visible that, with a 30% degree of ionization plasma, the total positive contribution to the first derivative is three times bigger than with a neutral gas.

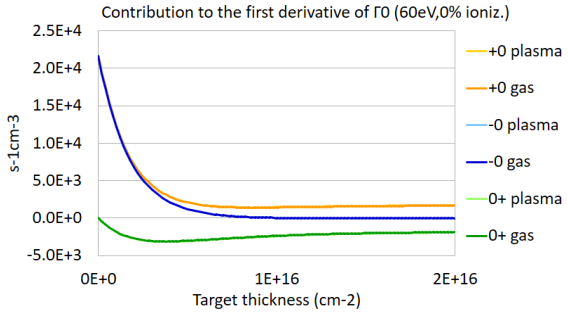

Figure 3.16: Contribution to first derivative of Γ^0 for a 60 keV beam on neutral gas

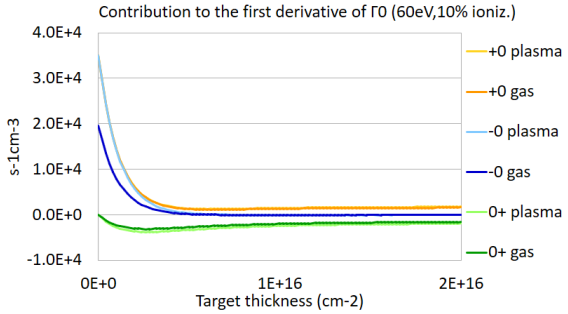

Figure 3.17: Contribution to first derivative of Γ^0 for a 60 keV beam on 10% degree of ionization plasma

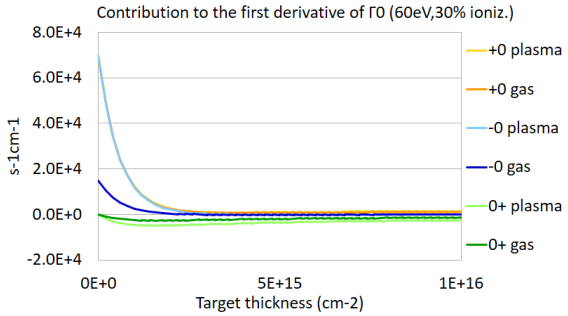

Figure 3.18: Contribution to first derivative of Γ^0 for a 60 keV beam on 30% degree of ionization plasma

Analogously the same graphics are produced for 200 keV and 1 MeV beam, the same trend for all energies considered is observed.

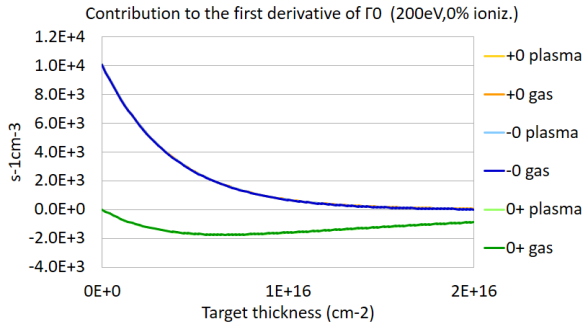

Figure 3.19: Contribution to first derivative of Γ^0 for a 200 keV beam on neutral gas

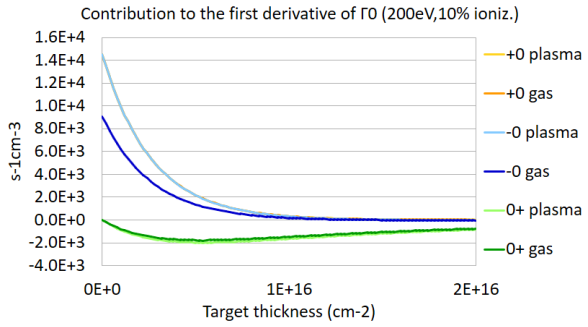

Figure 3.20: Contribution to first derivative of Γ^0 for a 200 keV beam on 10% degree of ionization plasma

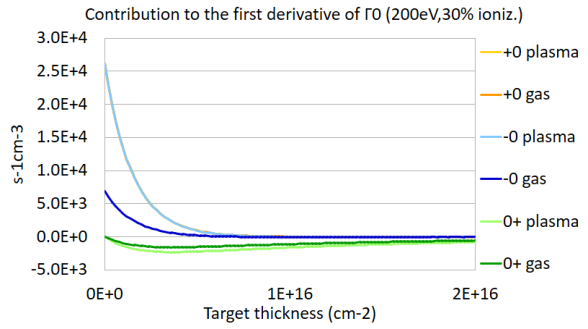

Figure 3.21: Contribution to first derivative of Γ^0 for a 200 keV beam on 30% degree of ionization plasma

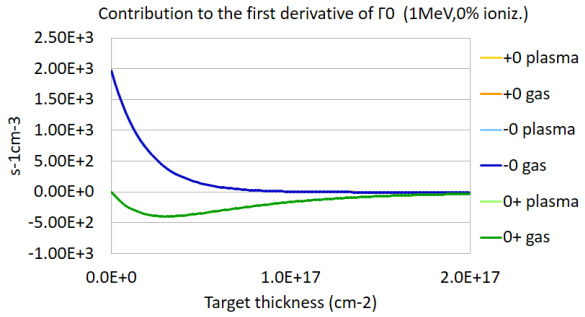

Figure 3.22: Contribution to first derivative of Γ^0 for a 1 MeV beam on neutral gas

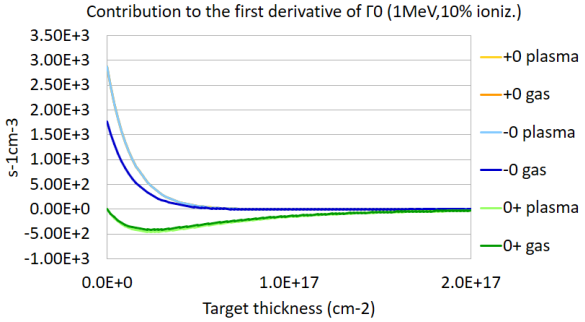

Figure 3.23: Contribution to first derivative of Γ^0 for a 1 MeV beam on 10% degree of ionization plasma

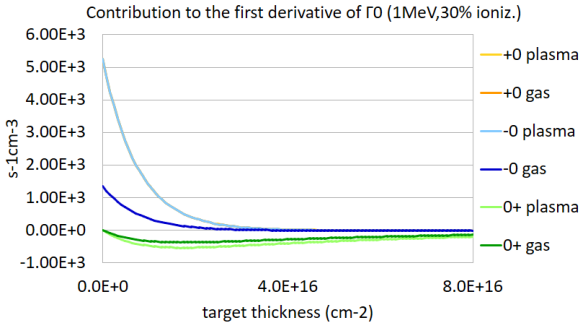

Figure 3.24: Contribution to first derivative of Γ^0 for a 1 MeV beam on 30% degree of ionization plasma

Chapter 4

Design of a beam-driven plasma neutralizer for NIO1

4.1 Description of NIO1

With the model of the neutralizer proposed in section 0.1 a minimum diameter for the neutralizer is needed in order not to loose the power of the beam directly to the neutralizer walls.
In table 4.1 the minimum diameter of the neutralizer is shown against distance from the source in the three different beam configurations exposed in section 0.1 .
The vacuum in the vessel will be kept by two cryogenic pumps with the nominal

distance	0.80	1.00	1.20	1.40	1.60	m	*total current*
1 beam	1.30	1.50	1.70	1.90	2.10	cm	14.4 mA
4 beams	4.12	4.32	4.52	4.72	4.92	cm	57.8 mA
9 beams	6.95	7.15	7.35	7.55	7.75	cm	130 mA

Table 4.1: Minimum diameter of the neutralizer

speed $R_s = 2000\ l/s$ and the capacity $Q = 900\ Pa\ m^3$.
The diameter and length of the vessel are respectively 0.35 m and 2 m. Each pipe going from the vessel to a pump has a diameter $d_p = 0.20$ m and a length of $l_p = 0.20$ m.
Here is a table summarizing all the dimensions of the system [8].

L	2	m
D	0.35	m
l_p	0.2	m
l_d	0.2	m
Q	900	Pam^3
R_s	2000	l/s

4.2 Neutralizer geometry

The geometry of the neutralizer-vessel system was shown in figure 5 while the gas flow was sketched in 1.2.
The gas will be supplied at the neutralizer center in order to mantain the chosen

target thickness along the path of the beam.
The diameter and length of the neutralizer will be determined by analytical study in section 4.3.
All the resistances of the system were calculated as the reciprocal of the respective conductances, calculated in section 1.4 and, with the geometry previously described, the electrical equivalent resistive system, shown in figure 4.1, is obtained.
The resistance beetwen P_2 and the "ground" is not $R_p + R_s$ but $\frac{R_p+R_s}{2}$ because,

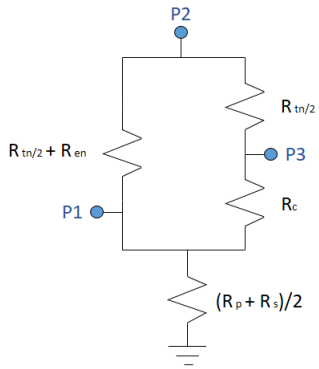

Figure 4.1: resistive system

as anticipated, the vacuum is mantained by two cryogenic pumps, halving the resistence there would have been with just one pump. With the resistive system shown in figure 4.1 the resistance seen beetwen p_2 and the "ground" is:

$$R_{eq} = \left(\frac{R_p + R_s}{2}\right) + \left[\left(R_{tn/2} + R_{et}\right) || \left(R_c + R_{tn/2}\right)\right] \tag{4.1}$$

4.3 Neutral gas flow and pressure profile

As anticipated in section 1.4, the conductance C of a channel, in molecular flow, does not depend on difference of pressure Δp but only on geometric propreties of the channels like length, diameter etc.; so equation 4.2 shows a linear dependence of flux on pressure.

$$F = C \cdot \Delta p \tag{4.2}$$

Equation 4.2 and the system shown in figure 4.1 link together the pressures in the different points of the neutralizer with the following equations:

$$p_2 = F_{tot} \cdot [(R_{n/2} + R_{ec} + R_c) || (R_{n/2} + R_{en}) + R_{ep} + R_p] \tag{4.3}$$

where F_{tot} is the total flux from the centre of the neutralizer to the pumps.

$$p_1 = F_{tot} \cdot (R_{n/2} + R_{en}) \tag{4.4}$$

$$p_3 = p_1 + (F_{tot} - \frac{p_2 - p_1}{R_{n/2} + R_{en}}) \cdot (R_{ec} + R_c) \tag{4.5}$$

There is still a degree of freedom that is the pressure at the center of the neutralizer p_2, to fix it, the target thickness is settled along the path of the beam to be $3 \cdot 10^{19} m^{-2}$: the target thickness required for the maximum efficiency for 60 keV

beam on a neutral gas, as computed in section 3.1.
With those formulas neutral gas density along the neutralizer was calculated for different configurations of the neutralizer in order to reach the previous target tickness at the end of the neutralizer.
In figure 4.2 density profiles are shown for different neutralizers. In this simulation a neutralizer of 1.30 m positioned 0.40 m far from the beginning of the vessel was used. Every two centimetres the density profile in neutralizers with diameters from 2 to 18 cm, was scanned.
In the figure diameter was reduced progressively from 18 cm (light blue line) to

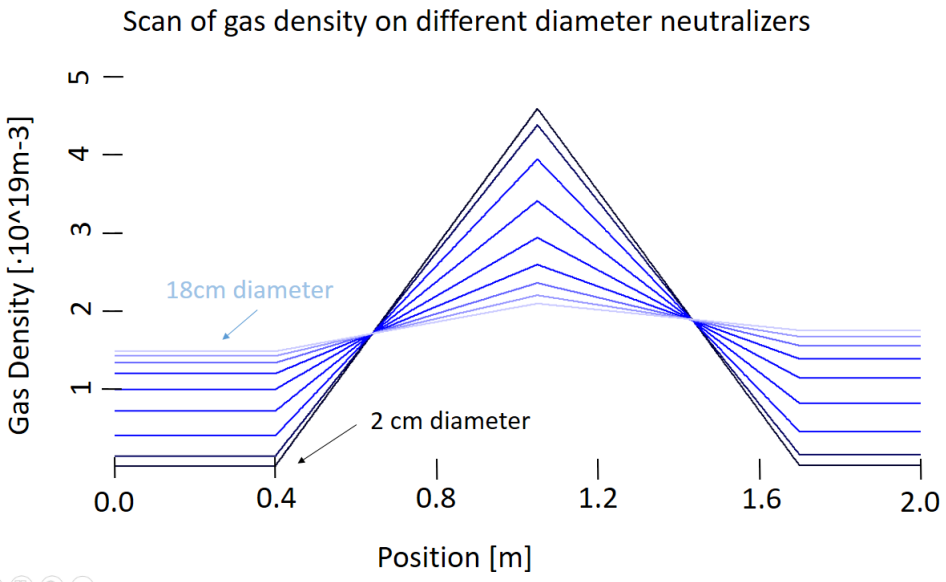

Figure 4.2: Density profile with different diameters

2 cm (black line). Gas density in the neutralizer increases with reducing of the diameter.
From figure 4.2 it is evident that a neutralizer with a smaller diameter confines the neutral gas better that a larger one, this is the reason why it will be chosen to reduce the radius of the neutralizer as much as possible.
A scan of the density profile was performed when changing the length of the neutralizer, in this simulation diameter was kept to 6 cm and the neutralizer was positioned 0.40 m far from the beginning of the vessel.
In figure 4.3 length was increased progressively from 0.6 m (light blue line) to 1.4 m (black line).
In the figure it is shown that the shorter the neutralizer, the higher the maximum of neutral gas density, but here the relevant quantity is not the maximum of neutral gas density but the target thickness of neutral gas inside the neutralizer:

$$tt_{in}^{g} = \int_{neut.begin}^{neut.end} n_{gas}(x)dx \tag{4.6}$$

that is proportional to the probability of ionization, inside the neutralizer, by a beam particle.
As previously said, a smaller radius neutralizer will ensure a higher gas density therefore, according to equation 1.6, a higher first ionization current I_{xb}. It is now time to decide whether better to use a smaller radius neutralizer, that will not

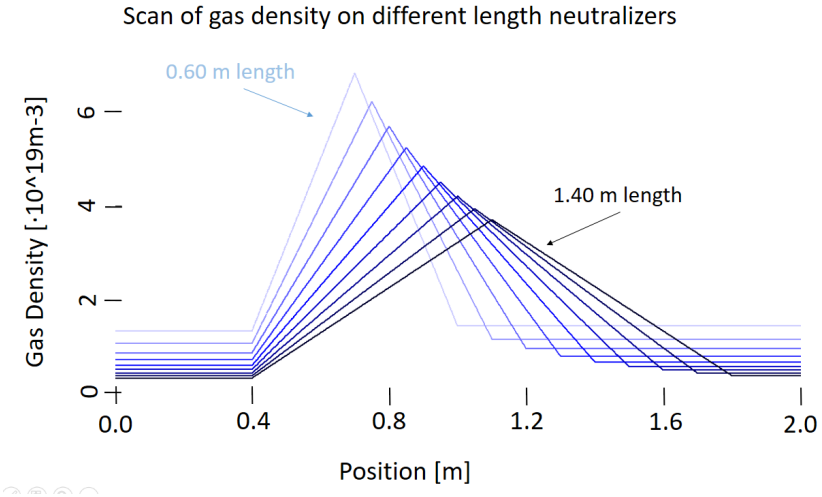

Figure 4.3: Density profile with different length

allow to use the 9 beamlet configuration, renouncing some power, or a larger one using all the power supplied.
Limits to the neutralizer radius are in table 4.1; according to the table and equation 1.6 the first ionization current for different configuration of the neutralizer was calculated and shown in figure .
Where the utilisation time is calculated with equation 1.26.
From figure 4.5 it is evident that the best configuration is that with a 8 cm diameter with all the power suplied.

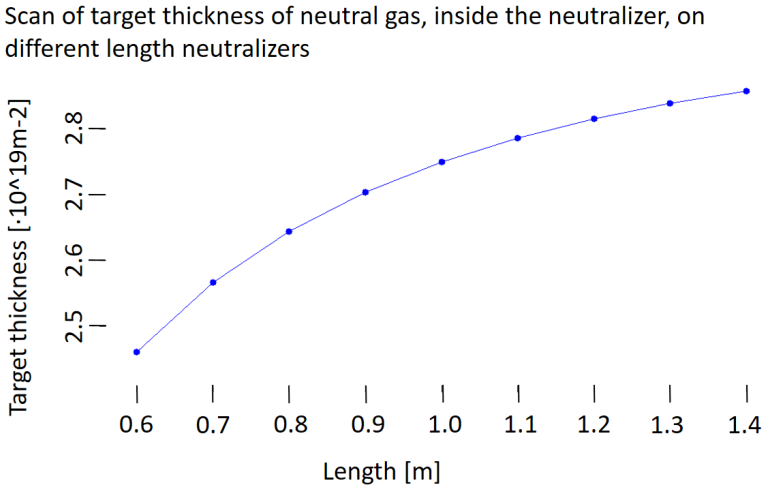

Figure 4.4: In the figure target thickness in the neutralizer for different length is shown, the targhet thickness in the neutralizer were calculated keeping constant the total target thickness, through the all path of the beam, to $3 \cdot 10^{19}\ m^{-2}$

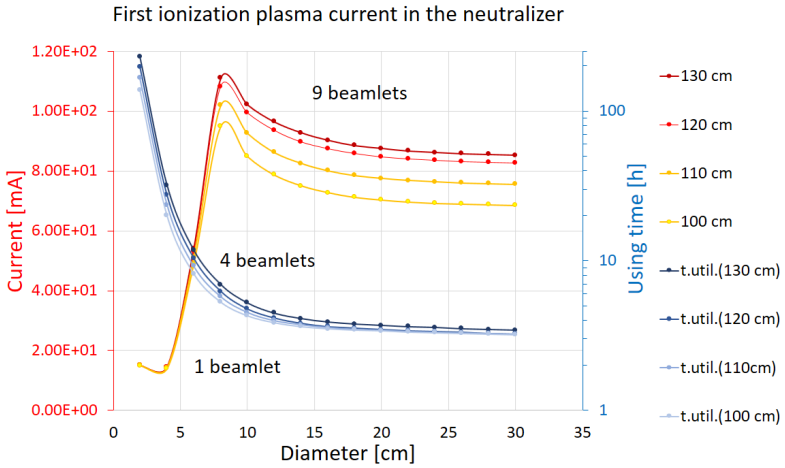

Figure 4.5: First ionization plasma current in different configurations neutralizers

4.4 Expected performances

This section will treat the expected performances of NIO1 neutralizer in different magnetic field configurations. Whit Changing the plasma confinement, the neutralizer length and target thickness, the best configuration of the neutralizer will be sought for, in order to reach the highest degree of ionization in the neutralizer.

4.4.1 Cusps magnetic field

To extimate the neutralizer efficiency plasma density in the neutralizer has to be found. Plasma density n_p will be calculated with equation 2.6.
As determined in section 4.3 the optimal neutralizer radius would be 4 cm. Due to lack of space (a neutralizer circumference of about 12.6 cm), the magnetic cusps will be produced by 6 magnets oround the neutralizer which should produce

a field of about 0.1 T. Calculating the leak width (w), with equation 2.7, the magnetic field is considered constant at the neutralizer border.
Al the quantities related with plasma generation, first ionization current, stripped electron current etc. were calculated along z axis. In this simulation beam current j_{beam} was assumed uniform on the radial and azimuthal coordinates, so the only coordinate which metters is the axial one z.
Nine simulations of plasma density were made with electron temperature $T_e = 10$ eV and ion temperature $T_i = 0.03$ eV, with changing the length of the neutralizer. Densities and ionization degrees were calculated for neutralizer from 0.60 m up to 1.40 m of length every 0.10 m.
In figure 4.6 neutral gas density and plasma density are shown. Neutral gas density is in blue, from light blue 0.60 m neutralizer, to dark blue 1.40 m neutralizer; while plasma density is in red, from light red 0.60 m neutralizer, to dark red 1.40 m neutralizer.
In figure 4.7 ionization degree is shown, with the previous convention: from light

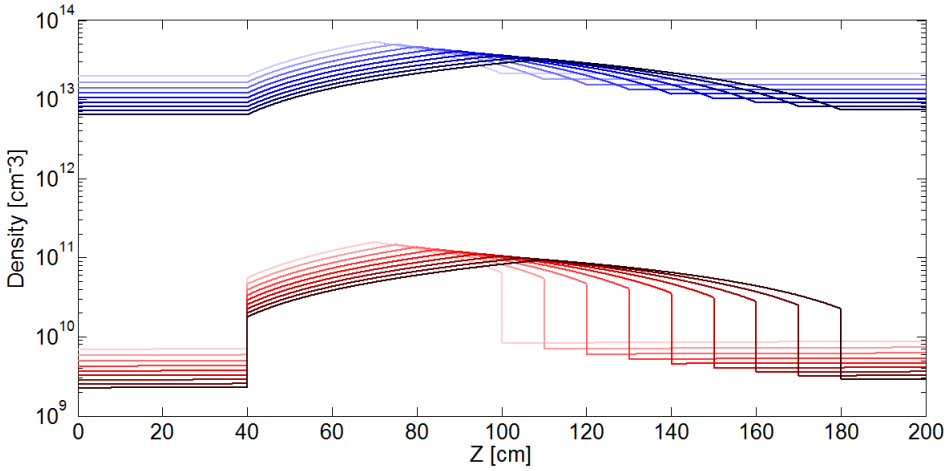

Figure 4.6: Neutral gas and plasma density

bluee 60 cm neutralizer, to dark bluee 140 cm neutralizer.
As it is shown in the figure, the maximum ionization degree in the neutralizer is

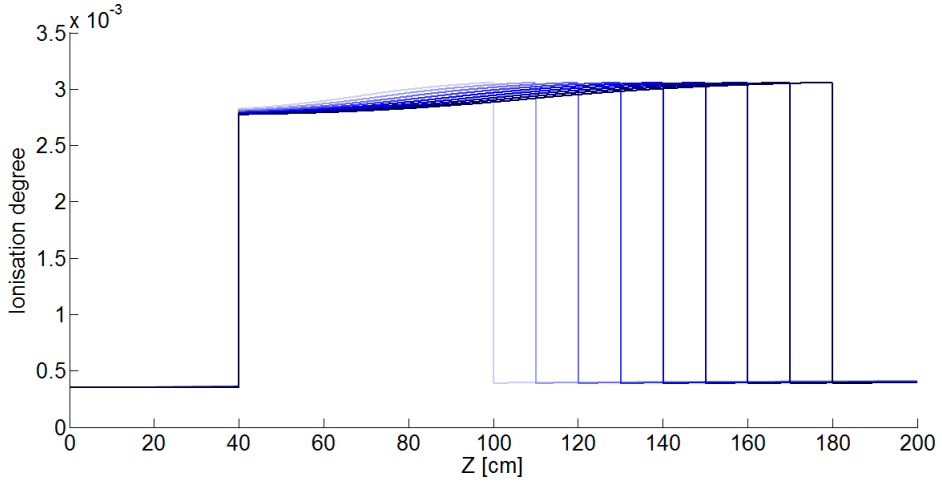

Figure 4.7: Ionization degree

less than 1%. A further comparison beetwen different length neutralizers is shown in figure 4.8.

The figure shows the maximum ionization degree, the maximum local plasma

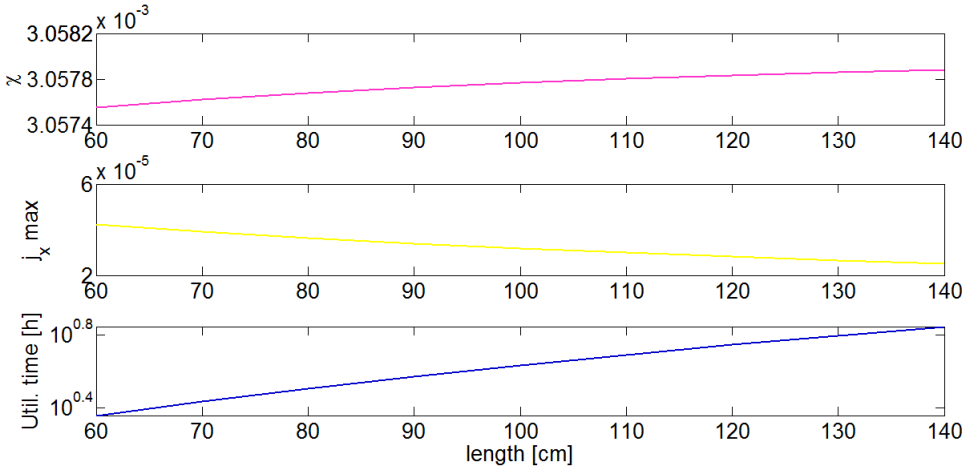

Figure 4.8: Comparison between parameters of different length neutralizers

current j_x and the utilization time for different length neutralizers. It is shown that the longer the neutralizer the higher the maximum plasma density; as predicted by equation 1.26 even utilization time encreases with increasing neutralizer length. Anyway from figure 4.8 it was found that a self powered plasma neutralizer, confined with magnetic cusps, will not be usefull for NIO1 beam.

With a ionization degree below 1% infact, the neutralizer efficiency will not increase significantly so as to be measurable.

Anyway in figure 4.9 the beam composition through the neutralizer is shown for different lengths. Whit the same convention as the previus figures the colors goes from light to dark in correspondence to simulations from 0.60 m to 1.40 m neutralizers. As in chapter 3 blue lines refer to Γ^0, red lines to Γ^+ and yellow lines to Γ^-.

In the figure it is shown that efficiency reaches about 65%, the same efficiency of neutral gas neutralizer.

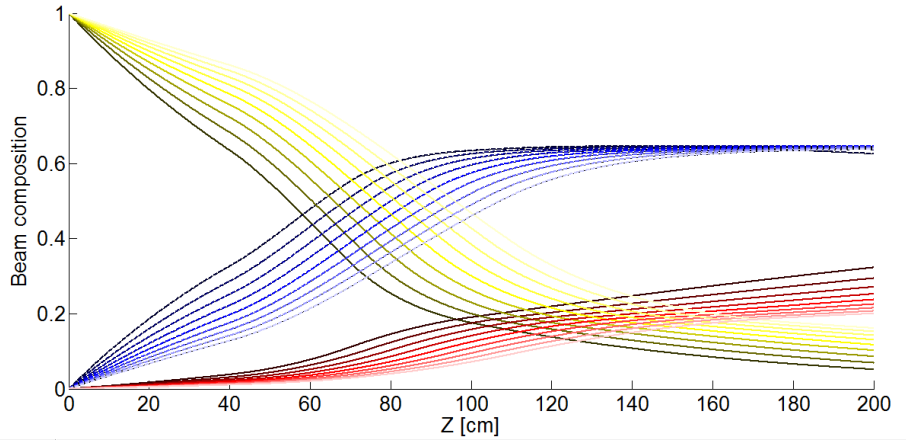

Figure 4.9: Beam composition for different length neutralizer

4.4.2 Axial magnetic field

As said in section 2.2, plasma confinement with axial magnetic field was studied thanks to a 2D model that quantifies plasma density $point - by - point$ in the neutralizer.
The regions of the vessel considered in the simulations will be those traversed by the beam: the neutralizer and the two zones of the vessel, before and after the neutralizer, that are within 4 cm from the axis of the neutralizer. According to what was found in section 4.3 4 cm is the optimal neutralizer radius for NIO1 beam features.
Beam current was approximated along the radius as a *sin-like* distribution which is 0 at border and has the maximum at the center. To be normalize to NIO1 current $I_{beam} = 0.130$ A, the beam current density $j_{beam}(r)$ was calculated as the following expression:

$$j_{beam}(r) = \begin{cases} \frac{I}{2\pi R_b^2} \frac{1}{1-\frac{8}{\pi^2}} \cos(\frac{\pi r}{2R_b}) & \text{if } r \leq R_b, \\ 0 & \text{if } r > R_b. \end{cases} \tag{4.7}$$

where R_b is the beam radius.
The beam width, in the 9 beamlets configuration, would be of of 3.3 cm at the

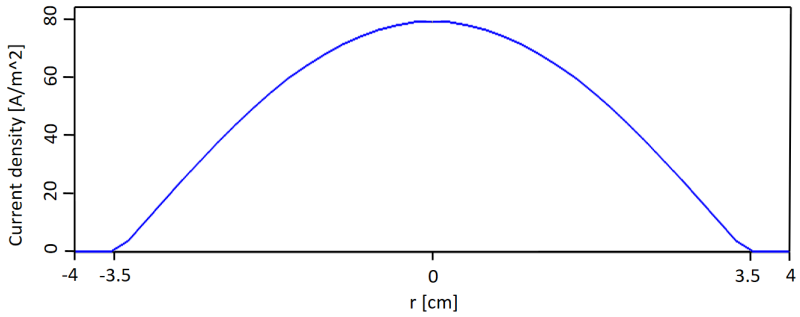

Figure 4.10: Current density of a 3.5 cm beam in a neutralizer of 4 cm

beginning and 3.9 cm at the end of the neutralizer, so a constant beam radius approximation, throughout the neutralizer, was chosen to simplify the calculation without loosing much information. The beam radius was approximated equal to 3.5 cm, as in figure 4.10.
Plasma density was calculated according to equation 2.22. In equation 2.22 plasma gain and loss: G and L were calculated according to equations 2.17 and 2.18; the electron temperature was approximated to 10 eV, while the ions are considered cold, 0.3 eV.
Neutral gas density was considered constant along radial coordinate and calculated along the axial one according to section 4.3, thus keeping the neutral gas target thickness after the neutralizer fixed to $3 \cdot 10^{19}$ m^{-2}.
The relaxation method, used to extimate the plasma density n_p, in these simulations was structured this way. Plasma density inside the neutralizer was initialized 0 m^{-3} at the first iteration; than, all the coefficients of equation 2.22 were calculated according to what previously said. Than Equation 2.22 was iterated 1000 times. After the first relaxation the entire cycle, calculations of coefficients and relaxation method of n_p, was repeated 100 times, with the new values of n_p found

in the previous cycle.
With this method four different simulations of plasma density were made.

Standard simulation

Firstly the case that, according to preliminary studies (section 4.3), is expected to ensure better perfonrmances was studied: a 1.30 m neutralizer with a 4 cm radius positioned 0.40 metres from the beginning of the vessel. With this configuration the pumps could work for about 6 hours before being regenerated.
Magnetic field is produced by a series of 100 coils each with the nominal current of 1000 A; to produce the magnetic mirror five coils are positioned at the two end of of the neutralizer.
Another approximation was needed due to a convergence problem of the algorithm. The force given by the gradient of $|\boldsymbol{B}|$, in formula $\boldsymbol{\nabla}|\boldsymbol{B}|N_a$, is very high, specally close to the magnetic mirrors, this makes the algorithm diverge. This is due to the approximation $\boldsymbol{\nabla}|\boldsymbol{B}| \parallel \hat{z}$ that is good inside the neutralizer but is no longer correct close the magnetic mirror where the radial component becomes bigger; this approximation overestimates plasma confinement of magnetic mirror. So, to avoid this convergence problem the value of $\boldsymbol{\nabla}|\boldsymbol{B}|N_a$ in modulus was *cut* to the maximum of 10^{14}.
Neutral gas density was calculated as in section 4.3, then the local value of n_p is subtracted to n_{gas}.
Plasma gain per second is shown in figure 4.12; it is shown that plasma gain is concentrated in the center where neutral gas density is higher. Anyway plasma gain in not symmetrical with respect to the center of the neutralizer; in the second half of the neutralizer infact, stripping electrons current is higher, so there the contribution of stripped electron to ionization is higher.
Plasma density is shown in figure 4.13. Outside the neutralizer plasma density was set equal to 0 m^{-3} because particles generated there would be lost following the magnetic lines to the wall of the vessel. Plasma density in the middle of the neutralizer reaches the value of $1.5 \cdot 10^{-17}$ m^{-3} a value that could be experimentally verified.
Figure 4.14 shows the ionization degree χ. As the figure shows, with this config-

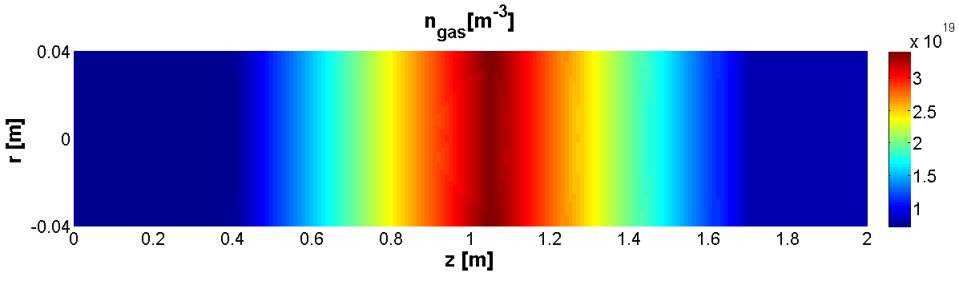

Figure 4.11: Neutral gas density

uration, ionization degree can only reach about 1%, not enough to appreciate the benefits of a plasma neutralizer on the neutralization efficiency.
It seems that for NIO1 a self powered plasma neutralizer would not generate enough plasma to optimize neutralization.
In figure 4.15 the neutral fraction of the beam Γ^0 at the end of the neutralizer is

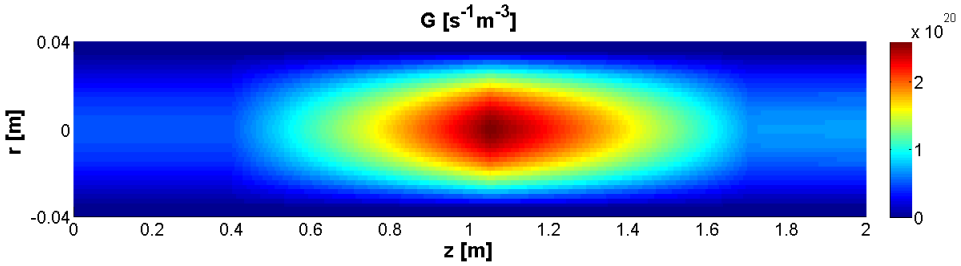

Figure 4.12: Plasma gain per second

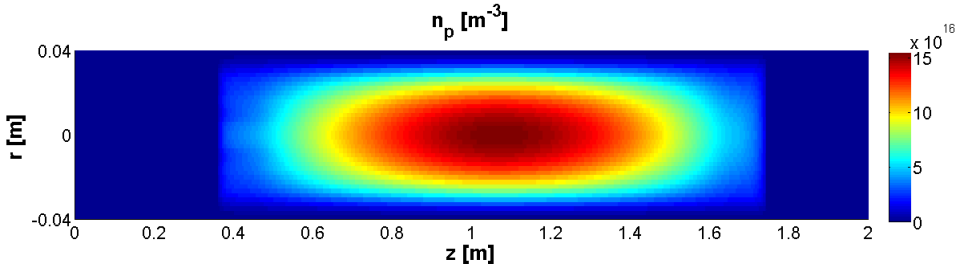

Figure 4.13: Plasma density

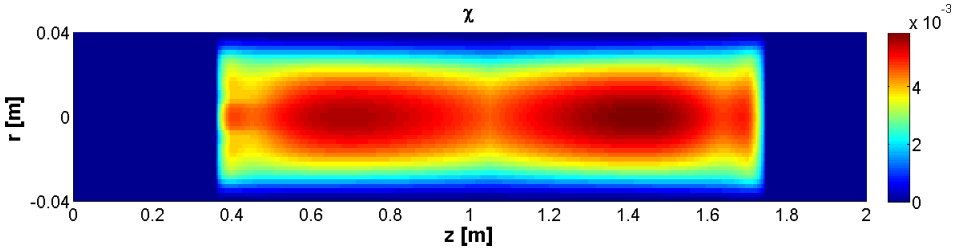

Figure 4.14: Ionization degree

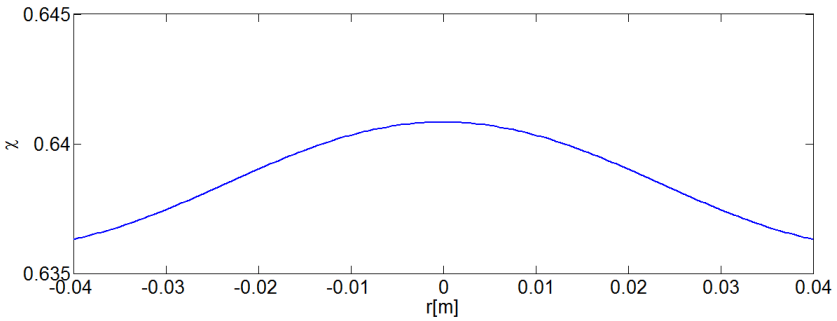

Figure 4.15: Neutralizer efficiency Γ^0 at the end of the neutralizer

shown; from the figure it is visible that close to the neutralizer axis, where the ionization degree is higher, the neutralizer is more efficient than at the border, where the beam traverses only neutral gas, but the difference is irrelevant. Plasma contribution increases neutralizer efficiency about 0.5 percentage point.

0.6 **m neutralizer**

The second simulation was made with a neutralizer with 0.60 m length, again with keeping constant the total target thickness at the end of the neutralizer.
In this configuration the system could operate for about 1 hour before having to

regerate the pumps, according to equation 1.26.
The magnetic confinement is provided by 46 coils instead of 100 due to the shorter length. For the same reason to produce the magnetic mirrors 3 coils were used at the beginning and at the end of the neutralizer.
With this configuration of the neutralizer almost the same ionization degree is reached as in the previous case. For this reason even neutralizer efficiency will be the same as in the previous case.

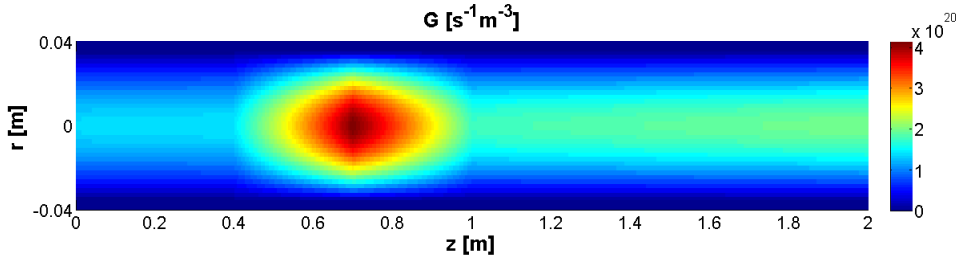

Figure 4.16: Plasma gain per second

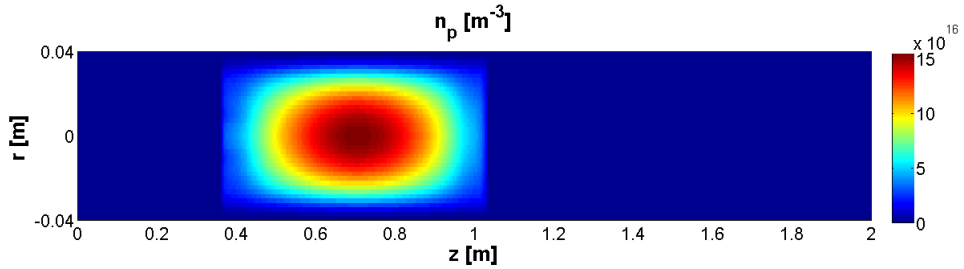

Figure 4.17: Plasma density

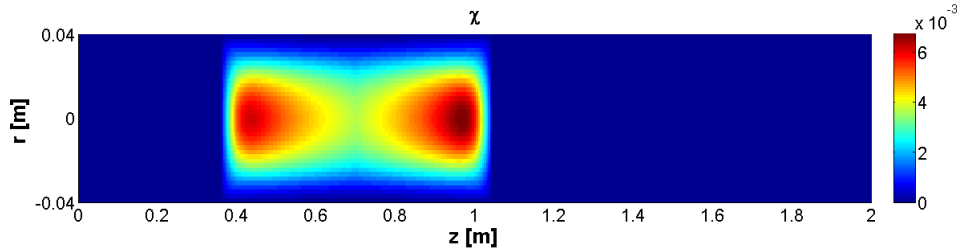

Figure 4.18: Ionization degree

5 **Ev electrons**

The case of colder electron plasma was studied. In this simulation the same configuration of the first simulation was used but changing the electron temperature, from 10 eV to 5 eV.
Results are shown with the same conventions as the previous simulations in figures 4.19, 4.20 and 4.21.

Not even in this simulation ionization degree gets higher; on the contrary it seems to be equal to that of the first simulations. Higher ionization degree was expected due to the lower diffusion of the cold electrons. Anyway recombination could cancel this positive aspect: cross section of recombination infact is higher for lower electron temperature, therefore the loss coefficient L will be higher.

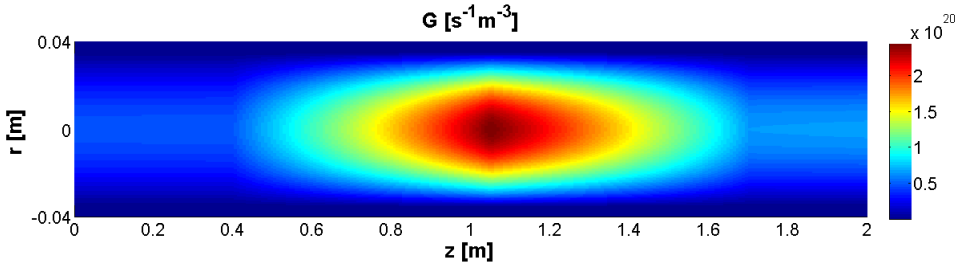

Figure 4.19: Plasma gain per second

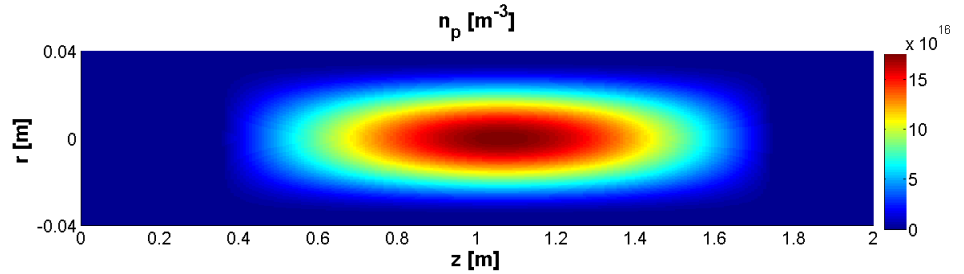

Figure 4.20: Plasma density

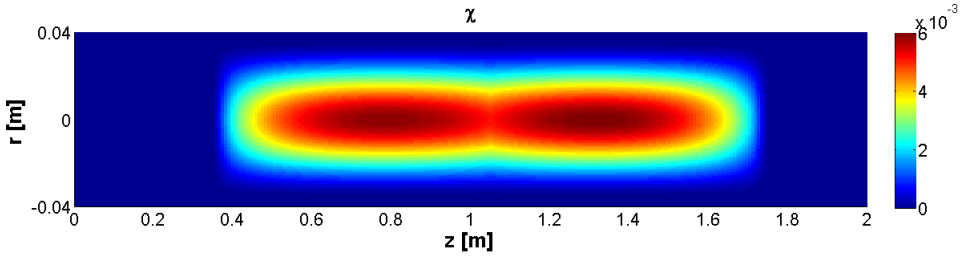

Figure 4.21: Ionization degree

With those three simulations it was demonstrated that for NIO1 a self powered plasma neutralizer would not generate enough plasma to achieve a relevant increase of neutralization efficiency.

In figure 4.22 a comparison beetwen degrees of ionization in the three con-

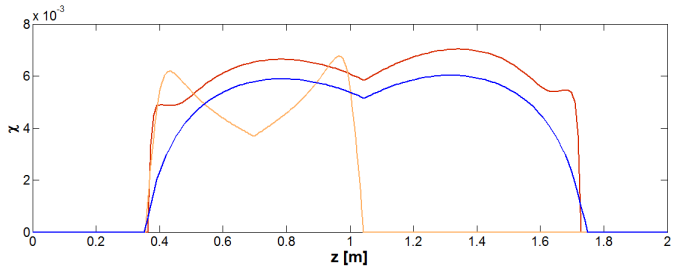

Figure 4.22: Longitudinal view of ionization degree on the axis of the neutralizer

siguration is shown. In the figure longitudinal view of ionization degree, on the neutralizer axis, in the three configurations, is shown. In the figure ionization degree of first simulation neutralizer, with 10 eV electrons is in red; ionization degree of the shorter neutralizer is the orange line, while degree of ionization obtained with the last simulation, with 5 eV electrons, is represented by the blue line.

A neutralizer in the first configuration guarantees higher ionization degree than other two.

0.39 **A beam current**

Whit the previous three simulations it was found that for NIO1 a self powered plasma neutralizer will not generate enough plasma; beam current infact does not guarantee enough ionization. The gain of plasma by primary ionization is proportional to the beam current, a higher beam current would generate more plasma in the neutralizer.
In this last simulation the same configuration as the first one will be kept but with three times as much total beam current, up to 0.39 A, to quantify if with a higher current would generate enough plasma to obtain significantly higher efficiency than with a neutral gas neutralizer.
Results are shown in figures 4.23, 4.24 and 4.25. Figure 4.25 shows that plasma

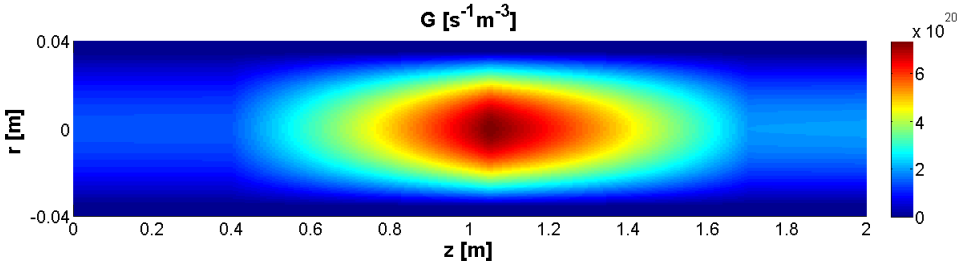

Figure 4.23: Plasma gain per second

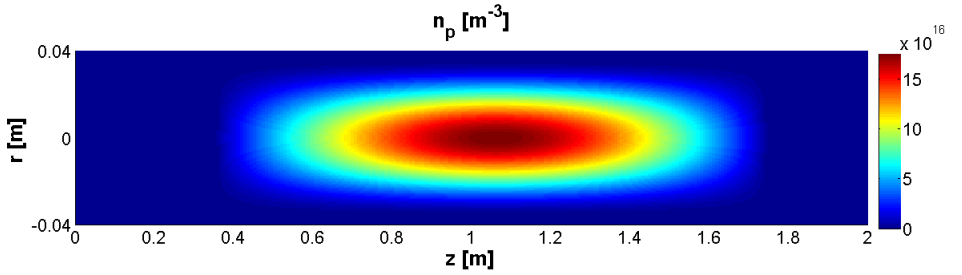

Figure 4.24: Plasma density

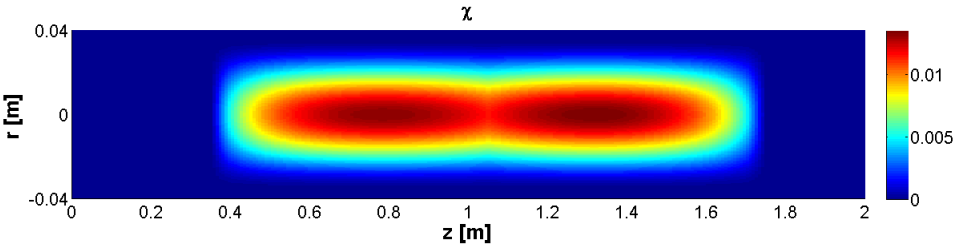

Figure 4.25: Ionization degree

degree of ionization reaches about 1.5%, so by tripling the beam corrent ionization degree is doubled.
In figure 4.26 the neutralization efficiency Γ^0 at the end of the plasma neutralizer is shown. From the figure it is visible that close to the neutralizer axis, where the ionization degree is higher, the neutralizer is more efficient than at the border, where the beam traverses only neutral gas, as in the first simulation. In

this simulation plasma contribution increases neutralization efficiency about 1 percentage points, twice the contribution of the first simulation.

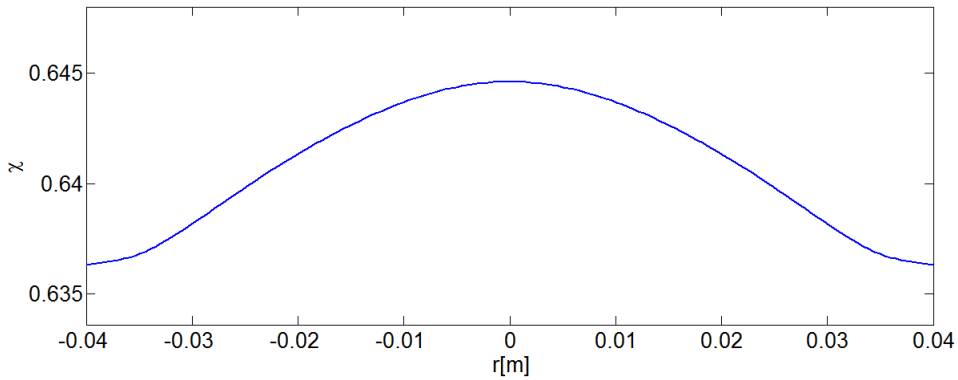

Figure 4.26: Neutralizer efficiency Γ^0 at the end of the neutralizer

Conclusions

Optimization of auxiliary heating systems will be crucial in future fusion plants. Among the major issues, this thesis is concerned with the efficiency of negative ion-based neutral beam injectors neutralizers.
Neutralization of three high energy negative ion beams was studied with an energy of 60 keV, 200 keV and 1 MeV. It was found that, for all three negative ion beams, a plasma neutralizer guarantees better efficiency than the usual neutral gas neutralizer.
The positive contribution of plasma to neutralization was quantified for all three beams and for different degrees of ionization of the plasma neutralizers. It was found that, for each energy considered, neutralization efficiency grows with increasing plasma degree of ionization, proving the possible relevance of plasma neutralizers in the controlled thermonuclear fusion panorama.
For a 60 keV beam, neutralization efficiency of a 30% degree ionization plasma neutralizer is extimed about 25 percentage points higher than the efficiency obtained with neutral gas neutralizer.
Prediction of the neutralizing model cosidered were successfully compared with experimental data for a 200 keV beam.
The most important neutralizing collisions of beam particles on plasma were studied to understand which collisions guarantee plasma neutralizers better efficiency than neutral gas neutralizers, finding that stripping reactions of negative beam particles on plasma are the main responsible for neutralization.
The subsequent step of this work was the design of a self powered plasma neutralizer for NIO1 negative ion beam source. A self powered plasma neutralizer does not require external plasma generation, plasma infact is generated by the beam itself with ionizing collisions with background gas.
Gas flux through NIO1 neutralizer-vessel system was studied with a lumped model in order to find the neutralizer configuration which guarantees higher neutral gas density in the neutralizer and so higher ionization probability by beam particles. It was valued that the smaller the neutralizer radius, the higher the gas density in the neutralizer, this with the condition of larger neutralizer radius than beam radius. Utilization time of the neutralizer-vessel model proposed was extimed of about six hours hours with cryogenic pumps.
With this purpose two different plasma confinement models were studied: magnetic cusps and magnetic coils. It was found that magnetic coils confinement guarantees higher plasma density than magnetic cusps.
It was demonstrated that for NIO1 beam a self powered plasma neutralizer is not configurable due to lack of beam current. Plasma degree of ionization infact is valued to reach about 1%.
Anyway a higher current beam could provide the density required to reach $10-20\%$ ionization degree thus increasing the neutralizer efficiency by almost the same

percentage without requiring any device for plasma production.
Plasma neutralizers will play a important role in optimizing neutral beam injectors efficiency; self powered plasma neutralizers could guarantee higher neutralization efficiency for high current beams as for the fusion demonstration reactor DEMO.
It is clear that a self powered plasma neutralizer will not work with NIO1 beam features because degree of ionization is insufficient to influence the neutralization efficiency. By contrast, if the plasma density can be increased by a dedicated plasma generator, test on neutralization with NIO1 will be made.
Neutralization efficiency could be compared for different degrees of ionization plasma.
In a larger scale, applying gas-beam interaction model to the DEMO neutral beam injectors plasma generation could be calculated.
The objective will be that of increasing negative ion neutralization reaching 80% efficiency with a self powered plasma neutralizers.

Bibliography

[1] Fusion Physics, International Atomic Energy Agency, Vienna, 2012.

[2] C.F. Barnett, Atomic Data for Fusion. Volume 1, (ORNL-6086),1990.

[3] P. Veltri, Lessons on ion sources, Course of Basic Plasma Physics, University of Padova, 2015-2016.

[4] M. Hanada, M. Kashiwagi, T. Inoue, K. Watanabe, and T. Imai. Experimental comparison between plasma and gas neutralization of high-energy negative ion beams, Review of Scientific Instruments, (75,1813), 2004.

[5] K.H. Berkner, R.V. Pyle, S.E. Savas and K.R. Stalder. Plasma neutralizers for H^- or D^- beams. Upton, NY, Oct. 1980,

[6] E. Surrey. Gas heating in the neutralizer of the ITER neutral beam injection systems, Nucl. Fusion (46), 2006.

[7] E. Surrey and A.Holmes, The beam driven plasma neutralizer, AIP Conference Proceedings (1515, 532), 2013.

[8] M. Cavenago et al,. Design of a versatile multiaperture negative ion source, Rewiew of Scientifin Instruments (81, 02A713), 2010.

[9] M. Cavenago et al., Status o f NIO1 construction, AIP Conf. Proc. 1390,640-649 (2011), American Institute of Physics, 2011.

[10] N. Fonnesu, M. Cavenago, G. Serianni, P. Veltri, Particle Transport and Heat Loads in NIO1, Oct. 2015.

[11] R.K. Janev, W.D. Langer, K. Evans Jr., D.E. Post Jr, Elementary Processes in Hydrogen-Helium Plasmas, Springer-Verlag, 1987.

[12] R.K. Janev, J.J. Smith, Review of Fundamental Processes and Applications of Atoms and Ions, World scientific publishing 1993.

[13] B. Ferrario, Introduzione alla tecnologia del vuoto, Patron Editore, Bologna, 1999.

[14] M. Liebermann, A. Lichtenberg, Principles of Plasma Discharges and Materials Processing, Wiley, May 2005.

[15] NRL plasma formulary. 2013. Naval Research Laboratory, Washington DC.

List of Tables

List of Figures